DEVELOPMENT OF A MICROFLUIDIC FLOW CYTOMETRY PLATFORM WITH FLUORESCENCE AND LIGHT SCATTERING DETECTION FOR THE RAPID CHARACTERIZATION OF CIRCULATING TUMOR CELLS

by

SAMANTHA ANN STEWART-JAMES

B.S., Minnesota State University Moorhead, 2012

A THESIS

submitted in partial fulfillment of the requirements for the degree

MASTER OF SCIENCE

Department of Chemistry
College of Arts and Sciences

KANSAS STATE UNIVERSITY
Manhattan, Kansas

2015

Approved by:

Major Professor
Dr. Christopher Culbertson

Copyright

Abstract

Circulating tumor cells (CTCs) have become a key component in the identification and treatment of cancer. Once dislodged from the main tumor, CTCs travel through the bloodstream and cause metastasis. Early detection and identification of these cells can help in the evaluation and prognosis of various types of cancer, as well as assisting in patient treatments by determining the spread of the disease. Here, a high-throughput microfluidic analysis technique is described that can efficiently detect and identify cells, with the specific identification of CTCs as a future application through fluorescent labeling in mind. As proof of principle, the device has been shown to detect and characterize individual human Jurkat (T-lymphocyte) cells at a rate of 100 cells/minute. The device employs micro-scale flow focusing to isolate individual cells. The cells are detected using both light scattering and laser-induced fluorescence to evaluate cell size and surface functionality.

Table of Contents

List of Figures

List of Tables

Acknowledgements

I would like to express my gratitude toward the Kansas State University Chemistry Department for the opportunity to study and perform my research in a supportive and caring environment. In particular I would like to recognize my advisor, Dr. Chris Culbertson, and thank him for his patience and guidance. Thanks also goes out to the members of my advisory committee: Dr. Dan Higgins and Dr. Jun Li. I am sincerely grateful for the lessons you taught me. In addition, I could not have completed my work without the help of Tobe Eggers and Ron Jackson. Thank you both for creating, repairing and modifying anything I ever needed.

My appreciation also goes out to those involved in the Kansas State University chapter of the NSF GK-12 fellowship program. In particular I'd like to thank the selection committee, Carolyn Ferguson, Kelly Dempewolf, and Teresa Woods for allowing me to be a part of this program, and Jen Sutter for welcoming me into her classroom. It has meant so much to me and truly helped me to grow as a scientist in my final year of graduate school.

I would also like to extend my thanks to my friends at K-State and beyond. In particular I would like to recognize Damith, Emery, Nicoleta, Chelsea, Katie, Nicole, and Julie. Thank you all for your help and support and for allowing me to discuss my research and thesis with you endlessly. You have made my experience here at K-State much more meaningful.

My deepest and most sincere appreciation goes out to my fiancé, Derrick Warnecke, without whose constant love, devotion and encouragement I would never have made it through. I am very lucky to be able to spend the rest of my life with such a wonderful man. The same depth of gratitude is also extended to my current and future family: Judy (and Richard) James, Candy Stewart-James, Roger Stewart, Katy Stewart-James, Dr. Nikki James, Yvonne (and Rolland) Johnson, Bob and Bonnie Warnecke, Greg and Patti Warnecke, Josh, Ashley and Liberty Essig, Michael Warnecke, and Haley Warnecke. Without all your love, support, and guidance I would not be where I am today. Thank you all from the bottom of my heart.

Most importantly, I would like to thank God. You are the true reason for my talents and success. Without your blessings I would have nothing. Every day I am reminded of your steady hand which helps to guide my life. Thank you.

Dedication

In memory of my grandfather, Dr. Richard Ernest James. You are the inspiration for the journey that led me to where I am today. Even now I look to you for the unconditional love and support you always gave freely. Your impact on those around you was great, and your influence on me was lasting. I hope to one day be the same guiding light to another as you were to me. Thank you for everything. I love you and miss you dearly.

"Ye whose hearts are fresh and simple,
Who have faith in God and Nature,
Who believe that in all ages
Every human heart is human,
That in even savage bosoms
There are longings, yearnings, strivings
For the good they comprehend not,
That the feeble hands and helpless,
Groping blindly in the darkness,
Touch God's right hand in that darkness
And are lifted up and strengthened;--
Listen to this simple story,
To this Song of Hiawatha!"

Excerpt from "The Song of Hiawatha" by Henry Wadsworth Longfellow[1]

Chapter 1 - INTRODUCTION

1.1 Microfluidic Flow Cytometry

1.1.1 Flow Cytometry

The basic principle of cytometry is to identify cell types in a given heterogeneous cell population. Flow cytometry advances this process by moving cells in a liquid stream past a detection system – usually a laser. Cell size and type can easily be distinguished using light scattering and fluorescence data, respectively. What began in 1954[2] with a simplistic instrument capable of determining cell count and size, has since grown into highly advanced and digitized instruments capable of detecting up to 13 different cell parameters[2] simultaneously.

The basic apparatus and mechanisms of an operating flow cytometry system are relatively simple. Cells are generally moved through a system using some type of hydraulic motion to move them toward the detector. One or more lasers are used to identify certain cell characteristics. Specific parts of a cell, such as the nucleus or cell membrane, can be selectively labeled using fluorescent dyes. The two most commonly utilized dyes are fluorescein and rhodamine (tetramethyl rhodamine isothiocyanate, TRITC), though many derivatives of these exist and are often much improved. Antibodies can also be fluorescently labeled and linked to specific cell surface receptors to be identified. The scattering of light off, and through, a cell can also provide useful information about the cell's characteristics. Forward-scattered light at angles from 0.5-10° and side-scattered light at 90° are indicative of cell size and granularity[2], respectively. These simple properties prove quite useful in the analysis of cells in a variety of scenarios and applications.

1.1.2 Flow Cytometry Applications

Flow cytometry has come a long way since the initial and simplistic measurement of cell size, now resulting in nearly 300,000 total references in SciFinder, and just under 20,000 in 2014

alone. Advancements in flow cytometry over the years have resulted in commercial instruments capable of detecting and characterizing cells at rates of up to 50,000 cells/min[3]. Although the measurement of cell size can prove very useful, flow cytometry now offers far more measureable parameters applicable to a variety of biomedical applications. These applications include the study of apoptosis through the measurement of caspase activity, DNA cleavage, mitochondria, the plasma membrane intactness, and cell viability[2]. One such study looked specifically at two proteins: cytochrome c (cyt c) and second mitochondrial activator of caspases/direct IAP binding protein with low PI (Smac/DIABLO). The main goal was to better understand the role they play in apoptosis via mitochondria permeabilization. Utilizing fluorescently tagged antibodies and flow cytometry, proteins were independently and simultaneously detected and tracked from the mitochondria to the cytoplasm, thus initiating the apoptosis cascade[4]. In a similar study, 7-Aminoactinomycin D (7-AAD) dye was used in order to study phagocytosis by differentiating the various stages of apoptotic cells via flow cytometry[5]. In more recent years, the combination of 7-AAD dye with various tagged antibodies has allowed the more specific steps a cell takes between complete viability and death to be identified[6]. These are just a few examples of the complex concepts which can be better understood through flow cytometry.

As more is understood about cell processes, the importance of flow cytometry in biological applications continues to increase. That said, the overall scope remains relatively narrow in the sense that the application is related primarily to cell process investigations wherein some type of cell fixation is utilized. These biological applications can, however, be extended or expanded to include and enhance research in the field of chemistry, incorporating a broader investigative scope to the technique of flow cytometry. Many of the simplistic techniques used to study basic cell functions have been adapted for studies in clinical laboratories[7], food and water analysis[8], and particle analysis[9] – including nanoparticles[10,11]. These assays have also been combined with analytical chemistry techniques such as mass spectroscopy[12] and microfluidics. The latter is the basis for the remainder of the discussion herein.

1.1.3 Microfluidics – Basics and General Principles

Microfluidics focuses on the precise manipulation of sub-nanoliter to nanoliter scale volumes of liquid, or sometimes gases. Although based on general fluidic principles, operations and interactions at this scale often differ from the macroscale. Most readily observable is the fact that the microscale system is far smaller. Therefore, the surface area-to-volume ratio is much larger. This also means that overall, the volume is not as impactful as the surface. Forces such as viscosity, electrostatic and electrodynamic interactions, and surface tension generally dominate[13]. Since these effects play a much larger role on the microscopic scale, careful consideration must be given to ensure that each is in balance with the others in order to achieve proper fluid, and sample, movement. Various ratios, displayed as dimensionless numbers, are often used to help gauge the overall function and effectiveness of a particular fluidic mechanism. They generally compare the competing surface and volumetric forces acting on a particular system. Examples of some of these numbers are shown in *Table 1.1*.

Table 1.1: Examples of various dimensionless numbers used to evaluate microfluidic mechanics[13].

Abbrev.	**Number**	**Description**	**Microscale**	**Macroscale**
Re	Reynolds Number	Inertial/Viscous	<2100	>4000
Pe	Péclet Number	Convection/Diffusion	10-200+	>1 ; <1
Pr	Prandtl Number	Momentum Diffusivity/Thermal Diffusivity	<1	0.004 - 100,000

The most important of these dimensionless numbers in regard to determining overall device function and design are the Reynold's number and the Péclet number. The Reynold's number provides information about the flow within the device – whether it is laminar or turbulent. The subject of laminar flow is discussed later on within this section. Generally in a microscale device the Reynold's number is less than one, which means flow is laminar, although as one can see from the table above, any ratio under 2100 would be indicative of laminar flow. This is

ideal since the flow can then be more precisely controlled and manipulated, as can the particles within the flow profile. The Péclet number provides a ratio to determine whether the dominate means of mass transport can be attributed to diffusion or convection. It is most useful in the determination of the length and width necessary in a microfluidic channel in order to achieve proper mixing. Generally speaking, diffusion is the dominant form of mass transport within microfluidic systems.

The Prandtl number is dependent upon the fluid viscosity and temperature. Since the area within a microfluidic channel is far smaller than on the macroscale (e.g. water ducts, pipes), the thermal diffusivity is higher, therefore causing a lower Prandtl number. Lower Prandtl numbers are indicative of large thermal boundary layers and small velocity boundary areas. Therefore, the heat will dissipate quickly from the channel to the surrounding thick outer layer. This allows for high voltage separations to be possible.

Another property of micro-scale fluid movement is the laminar flow profile, as previously mentioned. Working with fluids confined to micron (and sub-micron) scale spaces means that fluids will have greater interactions with channel walls. This means that interfacial interactions play a crucial role in determining how fluid will move at this scale. The condition at the interfacial boundary between the fluid and solid wall may discussed as a "slip or no-slip" interaction. Ideally, there would be complete slip of the fluid against the solid surface, creating a completely flat flow profile where the fluid velocity is equal across the entire fluid within the confined space. However, this type of profile is a highly idealized paradigm and unlikely to occur, except under conditions where electro-osmosis takes place. The strong influence of surface effects, including van der Waals forces, osmotic transport, porosity, and liquid evaporation, cause fluid to have a no slip, or partial slip, state against the solid wall. This phenomena can be observed in *Figure 1.1*[13] and is more commonly discussed in terms of laminar flow and a parabolic flow profile, shown in *Figure 1.2*. *Figure 1.1*[13] is a representation of the phenomena near the boundary. Across the channel, the flow is better represented in *Figure 1.2*.

Figure 1.1: Visual representation of slip vs. no-slip paradigm. Ls = slip length[13]

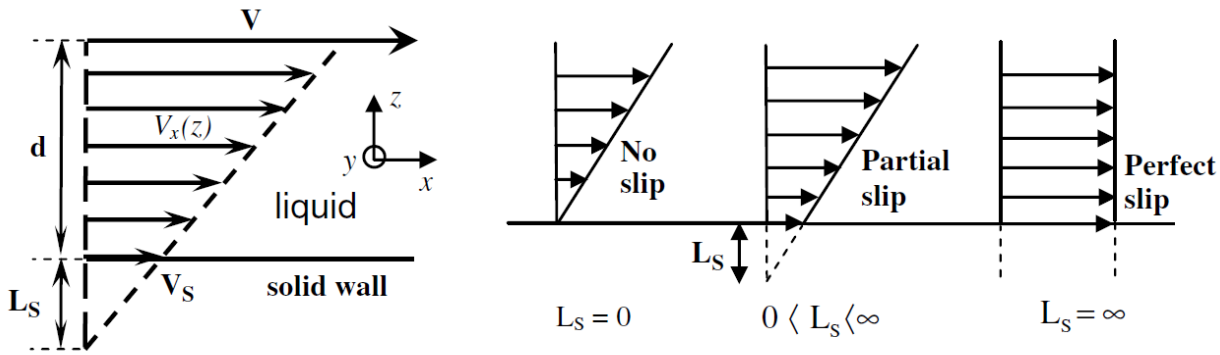

Figure 1.2: Visual representation of laminar flow and parabolic flow profile.

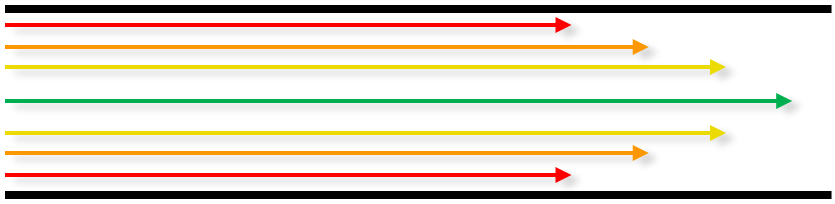

However, the van der Waals forces acting between the liquid and solid surfaces can be overcome by dramatically increasing the shear rates. Shear can be thought of as two layers of liquid passing against each other. The friction caused by these layers having contact during this movement is known as shear stress, and the amount of stress can change depending upon the liquid density. The shear rate is then simply the rate at which these liquids may deform during shear (i.e. shear deformation). The application of an appropriate pressure at one end of a channel can overcome this resistance and will generate a parabolic flow profile in the channel.

These basic fluid manipulations rely on various calculations to account for a multitude of parameters. This includes fluid resistance, velocity, momentum, stress and pressure, to name a few. In order to determine the correct parameters by which to create channels for proper fluid movement, the conditions listed must be carefully considered. The fluid resistance calculation is one of the most crucial, and has many factors for which to account – most significantly the sizes and shapes of the channels through which fluid will flow. For example, if one were to lay out a channel design without considering the effect of fluid resistance, it is likely that the fluid

would not flow in the intended direction, or the velocity would be slow. The resistance depends upon the lengths and widths of the channels in a manifold, as well as their cross-sectional shape. If a channel is too long or too narrow, or the shape is too broad or creates air space, the amount of fluid behind the pressure could be too great and the resistance will be too high, therefore effectively blocking the proper flow of fluid to that section of the device. Conversely, if one wished for flow to come from, but not into, a certain channel at an intersection this same technique could be applied to further control the movement of fluid and samples within the device.

For the applications discussed herein, fluid flow will be performed in semi-cylindrical channels. A representation of the fluid channel shape is demonstrated in *Figure 1.3*. A more in depth description of channel shape is discussed later in *section 2.1*, and a more accurate depiction is shown in *Figure 2.3*.

Figure 1.3: Representation of fluid channel (created using *Google SketchUp)*.

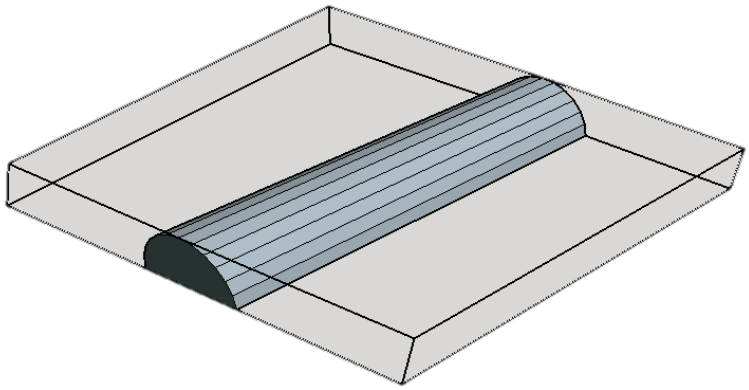

1.1.4 Microfluidic Flow Cytometry

Flow cytometry is utilized in many biological and biochemical applications. The miniaturization of flow cytometry using microfluidics has many significant advantages over its macroscale counterparts. Significantly, microfluidic flow cytometry devices are far smaller than bench-top

instruments and also have a more simplistic design and operating system. This means that they are easier to use and are more portable. In fact, microfluidic systems are currently in use for point-of-care analysis and monitoring of human immunodeficiency virus (HIV)[14] in remote areas where commercial flow cytometers are not practical. Their simple and cost efficient designs and fabrication techniques also mean that they can be incorporated into mass production lines, making them inexpensive to produce and potentially disposable. The small amounts of fluids used and narrow channels also allow for more precise control over the fluid flow profile, and therefore, over the sample within the fluid. Shown in *Figure 1.4* is an example of the narrow flow profile which can be created in a microfluidic device. This profile can be adjusted according to particle size to ensure single particle detection is achieved.

Figure 1.4: Focused flow profile of a microfluidic flow cytometry device.

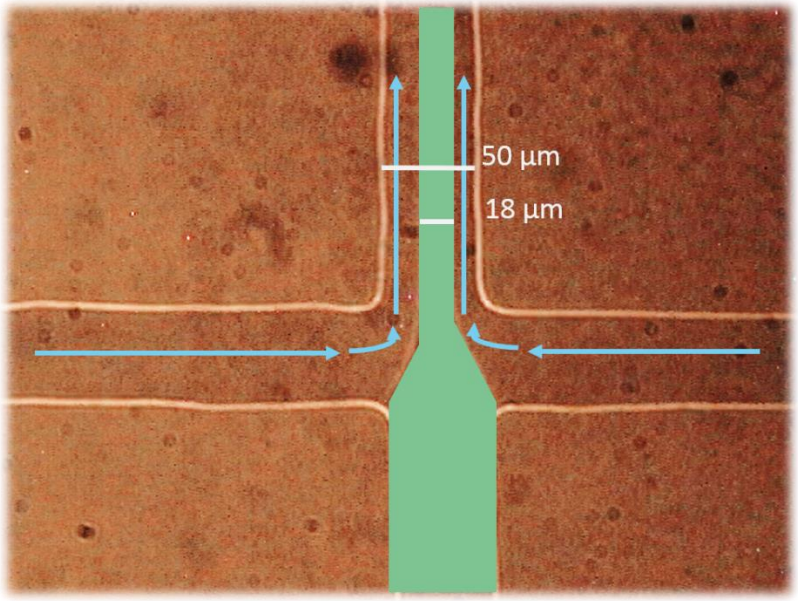

The ability to integrate several other upstream and downstream sample handling techniques makes microfluidic flow cytometry devices more efficient by reducing the amount of sample preparation and analysis time, and also reducing waste by consuming far smaller amounts of chemicals and requiring a smaller sample amount. They can also incorporate pre-concentration steps, effectively enriching the cell sample to make the detection of low sample concentrations more feasible. Techniques such as cell culturing and stimulation, mixing, cell lysis and

separation, and various types of cell assays can also be incorporated into a microfluidic device, creating a true micro-total-analysis system. This type of device integration not only means reduced time from sample to answer, but also a reduction in contamination due to less direct sampling handling steps. This provides a far cleaner and more pure sample, allowing more accurate and precise data and information to be obtained.

Overall, microfluidic devices provide more sensitive, selective, and repeatable results while still achieving similar detection speeds as commercial flow cytometers[3]. It has been shown that a single molecule of DNA 2kbp in length can be easily sized and sorted with only a sample size of 28 femtograms of DNA (a 375 femtoliter detection volume)[15]. The ability to perform quantitative and qualitative analysis of such small volumes is another major advantage to microfluidic devices over their macroscale counterparts. This small sample size also means reduced waste and more rapid analysis. Studies have shown that it is possible to perform a complete cell lysis with total separation in under 3 s[16]. These features combined also demonstrate the capability of high-throughput devices for a variety of applications.

Poulsen et. al.[17] displayed the ability to perform static and dynamic acute toxicity assays at a rate of 3 kHz with only a 30 s run time – effectively analyzing 10 cells/s. These results were also repeatable over multiple days and demonstrated the ability to detect cells at multiple time points. Repeatability is another benefit to microfluidics systems due to the higher degree of fluid handling precision. Stephen R. Quake has been a leader in the advancement of integrated valves to improve fluid pumping mechanisms and increase fluid handling precision. His push-down valve geometry[18] (shown in *Figure 1.5*) is a fully integrated on-chip pumping system and provides more direct and precise control over the pumping of fluid through the channels. This design has been particularly useful to the device described herein, and allows the ability to create better, faster flow rates and greater flow rate control versus off-chip pumping methods, such as an external syringe, which do not allow for minute changes in pumping pressure and sequence rates, and often cause air bubbles and may introduce contamination in some cases. The new on-chip pumping methods allow for the ability to construct very complex, multiplex

devices capable of individual control of over 1000 wells using only 20 control lines[19] – effectively creating a microfluidic circuit. These advanced microsystems are capable of performing high-throughput (over 1000 samples at once) screening assays, fluidic displays, and drug delivery implant systems with the potential to provide hassel-free long-term therapy, possibly replacing devices such as diabetic insulin pumps. These devices have also been shown to be capable of switchable bistable memory with metastatic flow states[20].

Figure 1.5: Stephen R. Quake push-down valve geometry[18].

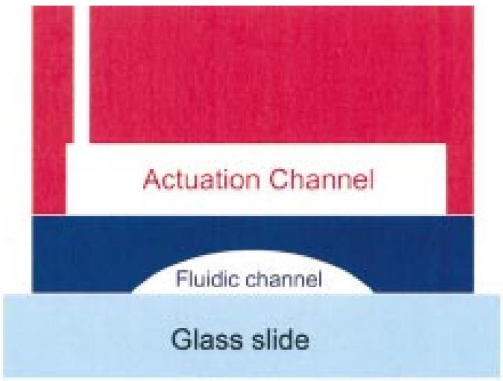

Multiplexed high-throughput devices such as these have allowed the screening of up to 5 million antibacterial biomolecule clones/day[21]. This type of high sample load and throughput shows it is possible to analyze millions of cells in a relatively short period of time, making the feat of finding a circulating tumor cell (CTC) of a density of one in a million a more achievable feat. It has already been demonstrated that 8 different biomarkers can be identified from a whole-blood sample after a 1-million-fold CTC enrichment via microfluidics, displaying a zero false-positive rate[22]. Better understanding of the principles behind rare-cell capture have allowed for more effective capture and enrichment of these types of analytes[23]. A centrifugal microfluidic device has also demonstrated the ability to perform rapid and effective enrichment of CTCs. The device demonstrates the ability to isolate and enumerate CTCs from whole blood within 30 s at high purity, showing capture efficiencies of up to 84%[24]. This shows great promise toward the development of a handheld point-of-care device for the collection and analysis of CTCs directly from patient whole-blood samples.

Although all these accomplishments are great leaps in the advancement of science, improvements can always be made. Many current devices generally employ external pumping mechanisms to induce fluid flow, such as a syringe pump. These systems, though an improvement over bench methods, can potentially introduce air bubbles or other contamination into the system by way of these external pumping mechanisms. Most also could use improvement in repeatability and precision of the pumping mechanisms. The devices and systems discussed previously also tend to focus on the lysis and separation of cells, or the study of bacteria, rather than focusing on a whole Eukaryotic cell – thus losing a large amount of "big picture" type information obtained from the study of whole animal-type cells. The device discussed herein utilizes ideas from past devices, while also improving upon them. The pumping mechanism is fully integrated on-chip to allow for more precise control of the fluid flow dynamics. This reduces the chance for air bubbles and also provides a more precise and repeatable method for controlling fluid flow. The device also displays the analysis of whole, un-lysed Eukaryotic and rare cells. This provides more complete information about the whole-cell characteristics and the ability to rapidly identify individual whole cells within a cell population. This requires less pre-processing and mimics a more in-vivo like scenario to more directly relate to human-based applications.

Overall, more can be learned about the properties and characteristics of individual cells, as well as determining the true heterogeneity or homogeneity within a particular cell population. This is especially useful in biological applications, such as identifying and characterizing circulating tumor cells within a heterogeneous cell population, when the accuracy of a reading can assist in early cancer detection and track metastasis, possibly saving a person's life.

1.2 Cell Basics[25]

This section will provide a basic review of cell biology. The general areas covered will be the cell membrane, cytoplasm, and nucleus. Please refer to *Figure 1.6* for a visual aid of all components described herein. Specific components of each described general area will be

covered within the section appropriate to the area of the cell in which they reside. This overview is not extensive, but simply meant to provide some basic background knowledge on the major components and functions involved within a cell. The focus will be a Eukaryotic cell, such as in humans and other animals.

Figure 1.6: Visual model representing a Eukaryotic cell[26].

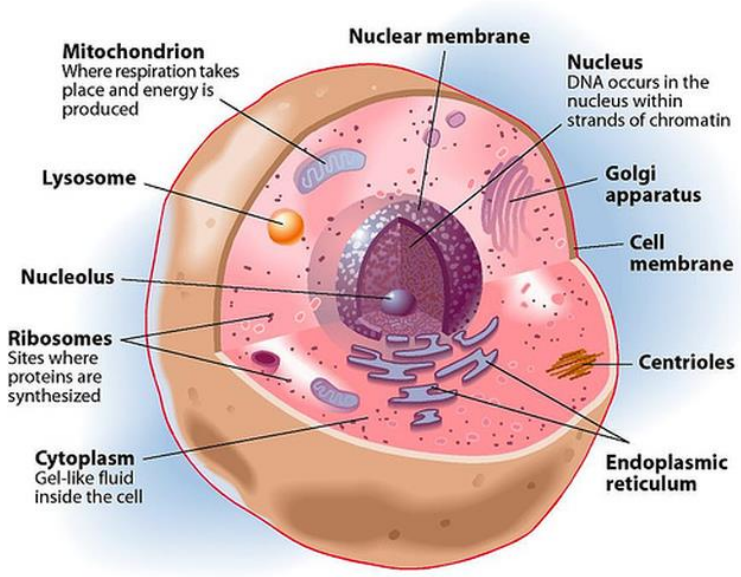

1.2.1 Cell Membrane

The cell membrane encompasses the entire body of the cell, effectively functioning as a protective sheath. It is composed of a phospholipid bilayer, as well as various proteins which function as selective gates. This allows the membrane to be semipermeable and allow selective movement of substances into and out of the cell. The cell membrane also contains markers for cell identification and recognition in the form of various surface molecules, such as glycolipids, glycoproteins and the like. Within the context of cytometry, it is the surface receptor proteins which are most important and allow for specific identification of cell types. Other major functions of the cell membrane include cell signaling, ion channel conductance, and cell adhesion.

1.2.2 Cytoplasm

Many of the cell's most recurring and important processes occur within the cytoplasm. This includes, but is not limited to, metabolism, replication, growth and cell expansion, along with various other protein cascades. It includes the entire area inside the cell membrane, except for the nuclear envelope which contains the nucleus, discussed later. Within the encompassing body of the cytoplasm lie many other important parts of the cell, including various organelles and other inclusions, in addition to the cytosol – the aqueous component of the cytoplasm which contains water and other ions, as well as some organic molecules. A large portion of the cellular processes mentioned earlier occur within this region of the cytoplasm. Prominent organelles included within the cytoplasm of a Eukaryotic cell are the endoplasmic reticulum, mitochondria, and Golgi apparatus.

1.2.2.1 Endoplasmic Reticulum

The endoplasmic reticulum has many different functions within the cell. It contains two parts – the rough endoplasmic reticulum (RER) and the smooth endoplasmic reticulum (SER). They are so named due to the many ribosomes on the RER, making the surface appear rough compared to the SER. The RER is involved with protein synthesis and secretion – such as for hormones, albumin, and milk. The SER is involved in synthesizing lipids, carbohydrate metabolism and metabolism of drugs and other foreign matter. However, the most consistent function of the SER is intracellular transport between the products it receives from the RER to their respective destinations in the cell – mainly the cell's sorting center: the Golgi apparatus.

1.2.2.2 Golgi Apparatus

The main function of the Golgi apparatus is to be a sorting center for the cell. It prepares and packages various proteins and other molecules within the cell for transport to their final destinations, such as the cell membrane or mitochondria, via glycosylation and formation of transport vesicles. It is also responsible for the creation of lysosomes, which contain enzymes necessary for various types of degradation within the cell.

1.2.2.3 Mitochondria

The mitochondria is the well-known cell "powerhouse," producing compounds such as adenosine triphosphate (ATP) responsible for the high amounts of energy necessary for many cellular processes. A majority of these energy-storing compounds are the product of cellular respiration, the process in which glucose is converted to ATP in the presence of oxygen, resulting in the production of water and carbon dioxide as waste products. The ATP created in the mitochondria is vital to a multitude of cell metabolic processes, such as those discussed in s*ection 1.2.2.1* on the endoplasmic reticulum.

1.2.3 Nucleus

Located within the nuclear envelope inside the cytoplasm, the nucleus is the key to the coding which determines the overall function of each individual cell. The chromosomes within this essential organelle contain the vital genetic material necessary for all cellular functions and reproduction. The three major parts – the nucleolus, chromatin, and nuclear envelope – are also essential to its function. The nucleolus is within the nucleus and contains the RNA and proteins and is responsible for the production of ribosomes via ribosomal RNA synthesis. Chromatin is also located inside the nucleus and is vital to its functions, particularly during cell division. It contains the nucleic acids and histones necessary to form chromosomes, which encode the functions of the next generation of cells and are responsible for gene expression. All these important components are enclosed within the nuclear envelope, the main function of which is to protect the nucleus and all it contains within a two-layered membrane composed of lipid bilayers, just as with the cell membrane. Nuclear pores allow highly controlled passage of certain particles and molecules, such as RNA and proteins, between the nucleus and the cytoplasm.

1.3 Circulating Tumor Cells (CTCs)

1.3.1 CTC Basics

The existence of circulating tumor cells (CTCs) has been known since the nineteenth century[27], but only recently have greater insights and promise been realized. CTCs are cells which have

been dislodged from an original, existing tumor site and circulate throughout the body via the circulatory system in peripheral blood[27-29]. It has been well established that they then reattach themselves in another part of the body, contributing to hematogenous metastasis[27]. Although they are rare at only approximately 1 in 100 million cells (though much higher concentrations are possible) in the bloodstream[27], their significance is great. Using microfluidics, the relative concentration can be increased since cells can be pre-processed prior to detection. CTCs have proven to be useful biomarkers for several diseases, including metastatic breast, colorectal, and prostate cancers[27-29]. Their ability to assist in early cancer detection and provide necessary prognostic information, particularly via simple liquid biopsy, has been clinically and analytically validated – and even approved by the United States Food and Drug Administration (FDA) for these purposes[28,29]. Several studies have shown a correlation between the presence of CTCs in the bloodstream and a patient's chance of relapse and/or survival[27-29]. Performing adjuvant chemotherapy after detection of CTCs has also been shown to eliminate CTCs in the blood and prevent metastasis[29].

However, CTCs have also been shown to be fairly fragile and have relatively short lifetimes[29]. Therefore, much improvement of current CTC testing methods is necessary to provide greater specificity and selectivity to improve upon the current false-positive rate of nearly five percent[29]. Still, it has been shown time and again that CTCs hold great promise for early cancer detection, as well as disease prognosis and insight into patient-tailored treatment methods. Current work with CTCs is focusing on identifying their specific biomarkers in order to assist in collaborative efforts to improve upon the selectivity and sensitivity of CTC detection. Dr. Anna Zolkiewska of Kansas State University (Manhattan, KS) and her team have made great strides in these efforts by identifying proteases within the ADAM (A Disintegrin And Metalloproteinase) family of proteases that show specificity in identifying breast cancer CTCs[30,31].

1.3.2 A Disintegrin And Metalloproteinase (ADAM) Family of Proteases

The ADAM (A Disintegrin and Metalloproteinase) family of proteases are transmembrane proteins generally located on the cell membrane, though some soluble forms have been discovered which can travel to other areas within the cell. Generally they are involved in

proteolysis and cell adhesion, though each have been shown to play very unique rolls. There are 21 members of the 40 total within this family that have been shown to be active in humans, and there has been a strong link shown between specific gene members and cancer. Specifically, ADAM9, 10, 12, 15, and 17 have been shown to have a strong correlation. In particular, ADAM 10 and 17 have been shown to promote cancer progression via both pathogenesis and carcinogenesis[32].

Due to their definitive and prominent role in the development and spread of cancer, the ADAM family of proteases make excellent biomarkers and can assist in diagnosis, prediction of patient outcomes, and treatment of cancer. The use of ADAM inhibitors has been shown to fight cancer and testing has already moved to clinical trials. Not all members of this protease family promote cancer, however. Many have other regular functions in the body such as sperm-egg fusion, sperm maturation, and oocyte recognition to promote conception. In fact, ADAM23 has actually been shown to help suppress tumors. Still, the function of some members of this family is yet unknown. Much work still needs to be done to better understand and utilize these proteases[32].

Dr. Anna Zolkiewska and her team from Kansas State University (Manhattan, KS) have been working on obtaining a better understanding, which is certainly needed, focusing much of their attention on ADAM12 – a proteolytically active member of the protease family, the function of which has been linked to the initiating of tumor formation and growth in breast cancer. There are several types of breast cancer, the tumors for each of these respond differently to various treatment methods and have very different overall patient outcomes. Zolkiewska and her team have been investigating several subtypes of the ADAM12 protease and have found a specific link between the splice ADAM12L and claudin-low (lacking the proteins necessary to maintain tight junctions and regulate molecule flow in the intercellular space between cells in the epithelium) tumors, which are attributed to breast-tumor initiating cells (BTICs) and generally exhibit aggressive characteristics, including resistance to neoadjuvant chemotherapy methods. Conversely, the splice variant ADAM12S has shown none of these same attributes[30,31]. The

work Zolkiewska and her team are doing allows for more specificity when identifying, and treating, breast cancer. This specificity can produce better biomarkers, allowing circulating breast tumor cells of a specific type to be easily identified within a heterogeneous cell population, aiding in patient diagnosis and treatment methods.

Chapter 2 - RESEARCH METHODOLOGY

2.1 Device Design

The device was designed using AutoCAD A360 software downloaded from Autodesk, Inc. The design for the device was chosen to be symmetrical and allow for narrow, even flow through the center of the analysis channel. Fluid channels were made longer to allow for any adjustments to be made later. Outer portions of the channel, for loading, were made to be 200µm wide. These channels then narrow to 50µm wide to create a narrow stream and allow for single cell analysis. Three outlets increase the overall flow, and therefore reduce the total analysis time and increase efficiency. The fluidic channel design is shown in *Figure 2.1(A)* and final modifications made to the design are shown in *Figure 2.1(B)*, with sample and run buffer loading channels stretching 1 cm from the channel cross.

Figure 2.1: Depiction of the (A) fluidic channel design, as well as the (B) final adjusted fluidic channel design used in device fabrication.

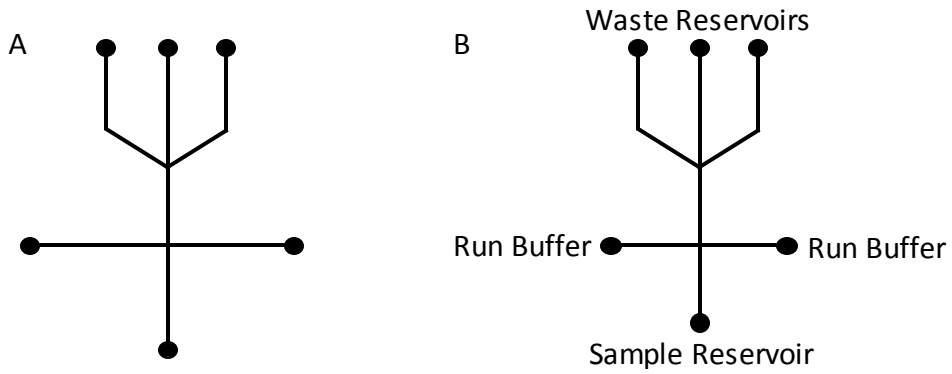

Air pumping channels were designed using an efficient three-valve layout. This reduced the overall cost by allowing a less expensive three-valve manifold to be used instead of the previous eight-valve manifold developed by another member of the group, Damith Randika. The cost was also reduced since fewer valves and less tubing were needed. Individual valves were designed for maximized for pumping efficiency at 400µm wide and 800µm long with 400µm vertical spacing and 800µm horizontal spacing between individual valves. The final design for the air-pumping (pneumatic) valves can be seen in *Figure 2.2*.

Figure 2.2: Depiction of final pneumatic valve design.

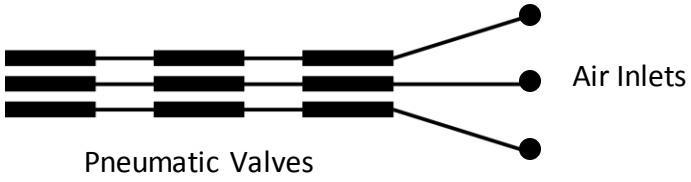

To assess the overall effectiveness of the design, the fluid resistance and flow rate calculations were carried out. Although channels appear hemispherical, they are not perfect hemispheres. In fact, a PDMS (polydimethylsiloxane) mold made from an AZ-P4620 master mold produces a chord (*Figure 2.3*).

Figure 2.3: Visual representation of the chord shape attributed to channels formed from an AZ-P4620 master mold.

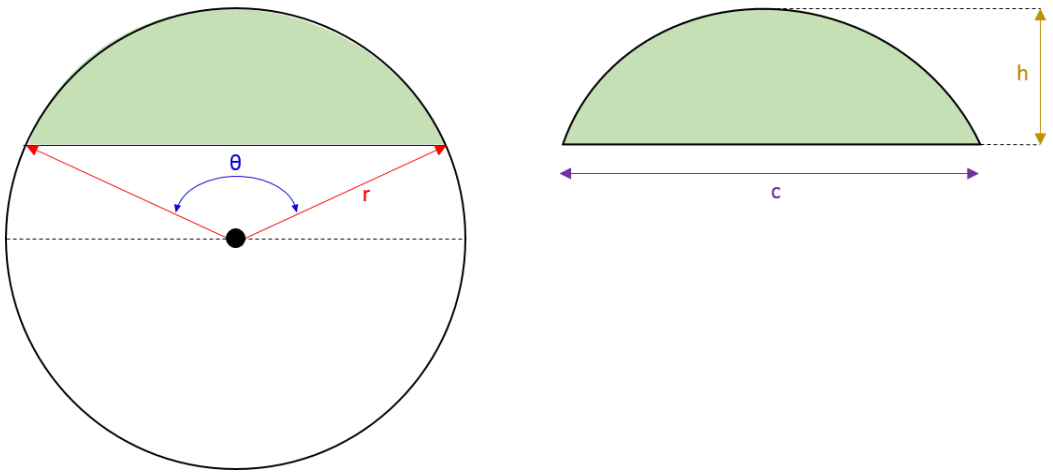

The volumetric flow rate is thus defined as:

$$V = Av \qquad \text{(Eq. 1)}$$

Where V represents the volumetric flow rate ($\mu m^3/s$), A represents the cross sectional area (μm^2) and v represents the linear velocity ($\mu m/s$). The cross-sectional area (A) of a chord is defined by:

$$A = \frac{r^2}{2(\Theta - \sin\Theta)} \quad \text{(Eq. 2)}$$

The variables are represented in *Figure 2.3*. The length and height of the chord are defined mathematically by:

$$l = 2r \sin\frac{\Theta}{2} \quad \text{(Eq. 3)}$$

$$h = r - \left[r^2 - \frac{l^2}{4}\right]^{1/2} \quad \text{(Eq. 4)}$$

Where l represents the length of the chord, *r* represents the chord radius, and *h* represents the chord height. This is a derivation of Poiseuille's Law:

$$V = -\frac{\pi}{8}\frac{r^4 \Delta P}{\eta L} \quad \text{(Eq. 5)}$$

Where ΔP represents change in pressure, η represents fluid viscosity, and *L* represents the total length of the tube, pipe or channel. Linear velocity, in the case of microfluidics, is calculated simply by:

$$v = \frac{dF_s}{F} \quad \text{(Eq. 6)}$$

Here, *d* represents the distance traveled by the sample, F_s represents the number of frames per second, and *F* represents the total number of frames. The fluid resistance calculations are just as important as flow rate calculations. Though it is beneficial to know how fast fluid will move inside a channel, and therefore how quickly samples will move past a detector in order to adjust the data acquisition rate accordingly, it is also necessary to know and understand where and how the fluid will flow to ensure samples are carried precisely and accurately in front of the

detection system in order to collect quality and reliable data. Total fluidic resistance is simply described as the drop in pressure over the volumetric flow rate.

$$R = \frac{\Delta P}{V} \quad \text{(Eq. 7)}$$

The change in pressure can be found by simply measuring the pressure difference from one end of the tube or channel to the other, or by using:

$$\Delta P = QR_h \quad \text{(Eq. 8)}$$

Where Q represents flow rate and R_h represents the total fluidic resistance. This equation is generally used for calculating blood flow in the body, but is applicable to flow for all smaller systems. For circular channels, total fluidic resistance is calculated by:

$$R_h = \frac{8\mu L}{\pi r^4} \quad \text{(Eq. 9)}$$

Where μ represents fluid viscosity, L represents total length of the tube or channel, and r represents the radius of the tube or channel. Simply, the total fluidic resistance (R_h) can be found by summing each resistance for each individual channel.

$$Channels\ in\ Series: R_h = R_1 + R_2 + R_3 + \cdots R_\infty \quad \text{(Eq. 10)}$$

$$Channels\ in\ Parallel: R_h = \frac{1}{R_1} + \frac{1}{R_2} + \frac{1}{R_3} + \cdots \frac{1}{R_\infty} \quad \text{(Eq. 11)}$$

For a better understanding of identifying channels in series or in parallel, see *Figure 2.4(A-B)*.

Figure 2.4: Representation of channels in (A) parallel and channels in (B) series.

A B

Based on these calculations, the device was designed using AutoCAD software and sent to be printed by Fine Line Imaging (Colorado Springs, Colorado). The fluid channels were printed using a positive photomask (colorless background with black features) to be used with AZ-P4620 positive photoresist. The air pumping channels were printed using a negative photomask (black background with colorless features) to be used with SU-8 2010 negative photoresist. Both masks are shown in *Figure 2.5(A-B)*.

Figure 2.5: Actual mask designs from AutoCAD software for (A) fluidic channels and (B) pneumatic actuation valves.

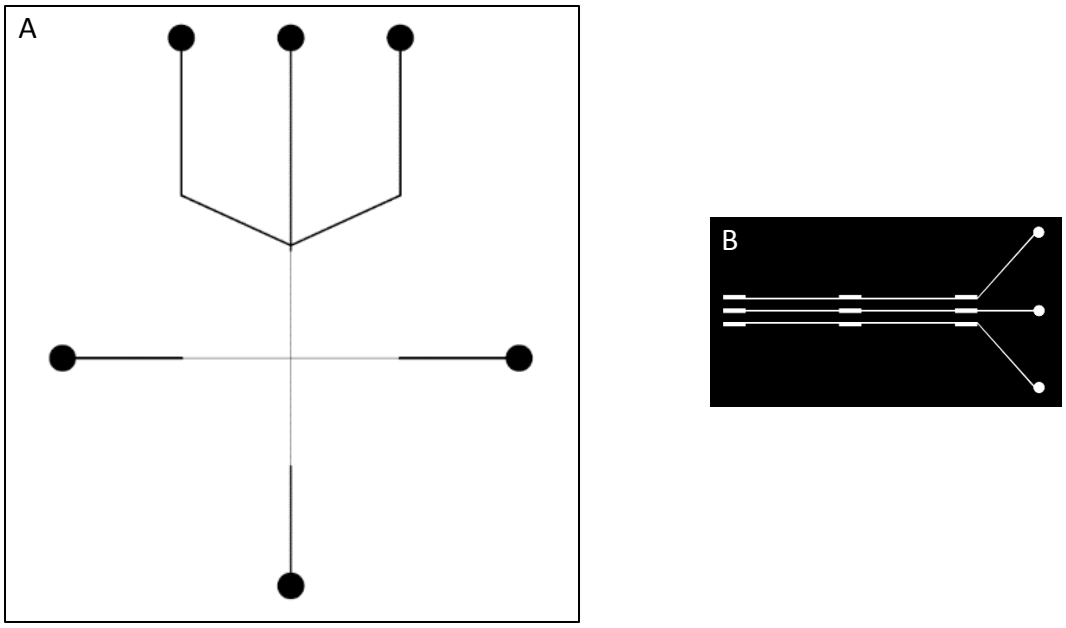

2.2 Materials

2.2.1 Software

AutoCAD A360 from Autodesk Inc. (San Rafael, CA) was used to create the pneumatic valve and fluid channel designs. Programs to control the microfluidic flow cytometry device flow and collect cell data were created and run using LabVIEW 2014, purchased from National Instruments (Austin, TX). Ambios Technology (Santa Cruz, CA) provided the software necessary to run the Ambios Tech surface profiling system used to characterize the surface of the AZ-

P4620 and SU-8 2010 master molds for the fluid channels and pneumatic valves, respectively. The Roxio VideoWave Movie Creator (Corel Corp. – Ottawa, Ontario, Canada) was used to record actual cell movement through the device in order to determine the flow rate and flow profile of cells within the microfluidic flow cytometry device. Data analysis of all runs was performed using IGOR Pro by Wavemetrics (Lake Oswego, OR).

2.2.2 Chemicals

Polydimethyl siloxane (PDMS) (Sylgard ® 184) was purchased from the Dow Corning Corporation (Midland, MI) to create the device molds for both the pneumatic valves and fluid channels. SU-8 2010 negative photoresist (Microchem Corporation – Newton, MA) was used to create the pneumatic valve master mold. Nitrogen flushed 2-(1-Methoxy) propyl acetate, 99% (Acrōs Organics – Fair Lawn, NJ) was used to develop the SU-8 2010 pneumatic valve master mold after exposure in the UV flood exposure system. Ethanol (190 proof) (Decon Laboratories, Inc. – King of Prussia, PA) was used to clean the glass slides and pneumatic valve master molds after creating a PDMS cast. Certified A.C.S. xylenes, for use in master mold channel protectant solution, and Certified A.C.S. Plus 2-propanol, for use in determining the stage of the SU-8 2010 pneumatic valve master mold development process, were both purchased from Fisher Scientific (Fair Lawn, NJ). Hexamethyldisilizane (HMDS) (Gelest Inc. – Morrisville, PA) was coated on the molds and served as a release agent, along with the xylenes. Sodium dodecyl sulfate (SDS) Reagent Plus™ ≥98.5% for use in the run buffer solution was obtained from Sigma-Aldrich (St. Louis, MO). Certified A.C.S. Sodium tetraborate and Fisher Biotech brand polyoxyethylene-20-Sorbitan Monolaurate (Tween 20) for use in the run buffer solution were obtained from Fisher Scientific (Fair Lawn, NJ). Compressed nitrogen gas for use in drying procedures and spin-coating was purchased from Matheson Tri-Gas, Inc. (Basking Ridge, NJ). An AZ-P4620 positive photoresist used to fabricate the fluid channel master mold was purchased from AZ Electronic Materials USA Corporation (Branchburg, NJ). The fluorescent labeling dye, 6-CFDA (6-Carboxyfluorescein diacetate) single isomer, was obtained from Biotium, Inc. (Hayward, CA) and used to fluorescently label Jurkat cells for on-chip microfluidic flow cytometric analysis.

2.2.3 Equipment

To reduce potential particulate contamination during microfluidic flow cytometry device assembly, a Labconco® (Kansas City, MO) Purifier™ Clean Bench and Horizontal Clean Bench were used. Clear "Magic Tape" from 3M (Saint Paul, Minnesota) was used to secure devices to the detection apparatus for cell analysis, and also to clean dust and debris from the PDMS devices and glass slides. The spin-coater used to produce photoresist-coated wafers was obtained from the Laurell Technology Corporation (North Wales, PA), model number WS-400A-6NPP/LITE. The UV flood exposure system for photoresist polymerization was purchased from Oriel Instruments (Newburyport, MA). Fisherbrand® 75x50x1.0mm plain microscope slides (precleaned) used to construct the microfluidic flow cytometry devices were purchased from Fisher Scientific (Fair Lawn, NJ), as were the Dry Bath Incubator (set to 37°C) and Marathon 8k centrifuge used for CTC and Jurkat cell preparation for analysis on-chip. Model Eclipse T5100 and model Eclipse TE 2000-U inverted microscopes both came from Nikon (Melville, NY) for the purpose of on-chip cell imaging. The solid-state 30 mW laser used to analyze CTCs was obtained from B&W Tek, Inc. (Newark, DE). The photomultiplier tubes used for both CTC and Jurkat cell analysis were purchased from Products for Research, Inc. (Danvers, MA). The 250mW ion laser and its power supply, used for Jurkat cell analysis, were purchased from Melles Griot Laser Group (Carlsbad, CA). To obtain on-chip videos of cell movement, a Sony (via the Sony Corporation of America, New York City, NY) Exwave HAD digital color video camera and EXFO (Quebec, Quebec, Canada) X-Cite® 120 Fluorescence Illumination System were used. To obtain accurate final channel dimensions from AZ-P4620 fluid channel and SU-8 2010 pneumatic valve master molds, an XP-2 surface profiler system from Ambios Technology (Santa Cruz, CA) was used. Cells were incubated using a Barnstead/Lab-Line (Melrose Park, IL) 120 Volt CO_2 Incubator. Mixing of the PBS/CFDA for cell uptake was done using a Fisher Scientific (Fair Lawn, NJ) Mini Vortexer. All oven baking steps performed at 80°C were done using a Lindberg Blue M (Ashville, NC) 120 Volt Mechanical Oven.

2.3 Device Fabrication

A typical multilayer soft lithography method was used to assemble all microfluidic flow cytometry devices[33,34]. Two master molds were used – one for creating a cast of the fluidic

channels, and another to create a cast of the integrated pneumatic actuation valves. The use of a multilayer device with an integrated pumping mechanism allows for more precise control of pneumatic pumping allowing elevated precision for the narrowing of sample flow, and also decreases the formation of air bubbles on-chip. This creates a more accurate and precise analysis of individual cells on-chip.

2.3.1 Fluid Channel Master Mold Fabrication

The fluid channel master mold was made using AZ-P4620 positive photoresist in order to create the chord-shaped channels necessary to allow a full seal of fluid channels for pneumatic pumping mechanisms to occur. The AZ-P4620 positive photoresist was stored at 4°C. Thus, the photoresist was removed from the 4°C refrigerator and allowed to warm to room temperature (~22°C). In the meantime, a new chromium-coated silicon wafer was rinsed with 18 MOhm water and dried with nitrogen gas at a pressure of ~150 kPa. Once the positive photoresist had come to room temperature, approximately 3-4 mL was spin-coated onto the chromium-coated silicon wafer under nitrogen gas at 1000 rpm (1270 rpm/s) for 17 seconds. The chromium-coated wafer ensured better adhesion between the photoresist and the wafer, thus allowing for a simpler development process later on. The wafer was baked at 70°C for 1 min, then the temperature was ramped up at a rate of approximately 47°C/min to 95°C. Once the temperature came to 95°C it was held there for 1 min. The temperature was ramped up again at a rate of approximately 47°C/min, this time to 120°C. Once the final temperature reached 120°C it was held constant for 2 min. The wafer was removed from the hot plate and placed under a watch glass (due to AZ-P4620 moisture sensitivity) on the bench top at room temperature (~22°C) for 20 min. *Figure 2.6* provides a visual representation of the temperature programming process.

Figure 2.6: Visual representation of temperature programming for bake time during AZ-P4620 fluid channel master mold fabrication.

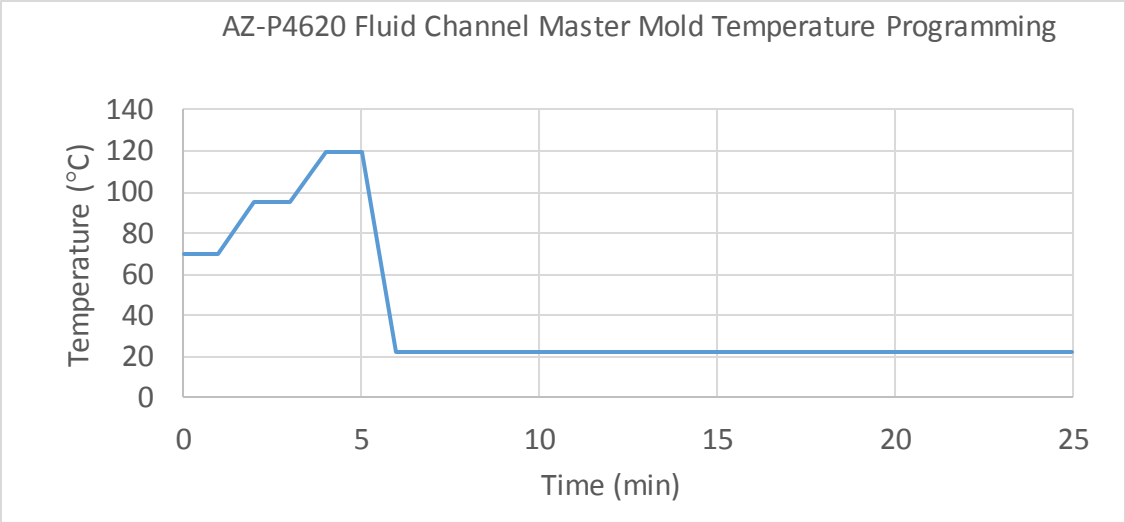

Next, the mask shown in *Figure 2.5A* was placed onto the AZ-P4620 positive photoresist-covered chromium-coated silicon wafer and covered with a cardboard frame (to allow better alignment later) and a quartz glass block. See *Figure 2.7* for a visual representation of this setup.

Figure 2.7: Model displaying setup used for UV flood exposure to create desired design on photoresist-coated silicon wafer.

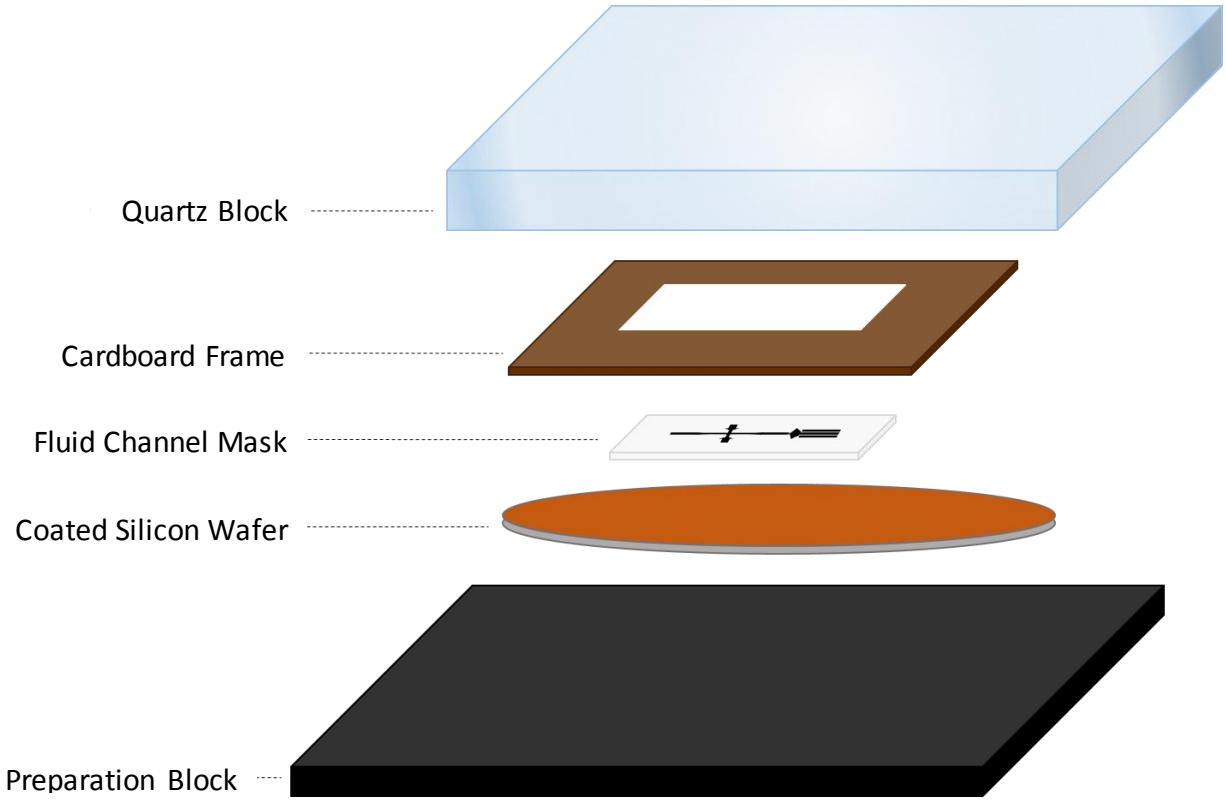

The wafer was then exposed to ultraviolet (UV) light using a flood exposure system at 500 mW and ~32 µW/cm^2 for 26.00 s. The wafer was allowed to rest for ~30 s in the flood exposure system immediately following the exposure time to allow it to cool. The wafer was then cooled further to room temperature (~22°C) under a watch glass on the bench top for an additional 10 min. Once fully cooled to room temperature, the wafer was developed carefully, gently and without agitation in a solution of 1:4 AZ 400K Developing Solution (i.e. Potassium borates). When all the exposed photoresist had been removed from the wafer and the exposed portion was again 100% reflective and only the channel design remained, the wafer was rinsed gently (water stream was not directly on the fragile channels) with 18 MOhm water. The wafer was carefully dried with nitrogen gas using ~25 kPa of pressure. When not in use, the wafer was stored on fiber-free cloth in a covered plastic petri dish inside a lab drawer at room temperature (~22°C).

2.3.2 Pneumatic Actuation Valve Master Mold Fabrication

The pneumatic actuation valve master mold was created using SU-8 negative photoresist. The negative photoresist was spin-coated onto a silicon wafer (uncoated) for 45 s at 1000 rpm (1270 rpm/s). The silicon wafer spin-coated with SU-8 2010 negative photoresist was soft baked for 2 min at 65°C, then immediately moved to 95°C and held there for 4 min. The wafer was cooled to room temperature (~22°C). The pneumatic actuation valve mask shown in *Figure 2.5B* was laid onto the wafer and covered with a cardboard frame and quartz glass block in the same manner shown in *Figure 2.7*. The wafer was exposed to UV light using the same UV flood exposure system described previously for 5.40 s at 500 mW and ~32 $\mu W/cm^2$. The wafer was allowed to rest in the flood exposure chamber for ~30 sec immediately following the exposure time, hard baked at 65°C for 2 min, then immediately moved to 95°C and held there for 4 min, and finally allowed to cool to room temperature (~22°C). The master mold was developed with slight agitation using 2(1-methoxy) propylacetate. The state of the development process was checked periodically (approximately every 1-2 min) by rinsing the wafer with isopropyl alcohol. If a white residue appeared, the wafer was returned to the developing solution. When no white residue appeared after rinsing with isopropyl alcohol, the wafer was dried using nitrogen gas at a pressure less than 50 kPa. When not in use, the wafer was stored in the same manner as described previously for the AZ-P4620 fluidic channel master mold.

2.3.3 Polydimethyl siloxane (PDMS) Preparation

Three different ratios of polydimethyl siloxane (PDMS) were prepared in order to fabricate the multilayer microfluidic flow cytometry device. A more flexible 30:1 (Sylgard base to Sylgard curing agent) ratio was used for the fluidic channel cast, while more rigid 5:1 and 10:1 ratios were used for the pneumatic valves. This ensures full pneumatic function (fluid channel closure) to pump fluid through the device, as well as complete cross-linking between the fluidic and actuation channel layers. In order to conserve materials and reduce cost and waste, the minimum amount of base and curing agent was used in order to achieve proper device fabrication. The base and curing agent come in a kit designed to make 10:1 ratios of PDMS. Therefore, making other ratios of PDMS can often become wasteful since the two components

will not create the same number of fabrications. This is why the ratios are fabricated in the manner shown below – to allow for minimal waste by maintaining an overall 10:1 ratio between each of the fabricated PDMS ratios. The amounts of base and curing agent for each ratio are shown in *Table 2.1*, along with the total amounts used for each. Each ratio was mixed thoroughly for 1-2 minutes before being degassed for approximately 20-30 minutes. The approximate 10:1 ratio was simply used as a filler after the essential ratios of 30:1 and 5:1 had been poured. The larger the difference between the ratios, the greater the amount of cross-linking.

Table 2.1: PDMS ratio amounts used to conserve materials.

	Base	***Curing Agent***
30:1	6.00 g	0.20 g
≈10:1	25.00 g	2.30 g
5:1	6.00 g	1.20 g
Total Amount	**37.00 g**	**3.70 g**

2.3.4 Multilayer Microfluidic Flow Cytometry Device Assembly

In order to prevent damaging the channels and valves of the master molds, a 1:1 solution of hexamethyldisilizane (HMDS) and xylenes was applied to the wafers prior to forming a cast with PDMS. One to two drops of the HMDS:Xylenes mixture was applied to the SU-8 2010 pneumatic actuation valve wafer to completely coat the valves and channels. The wafer was tilted and rotated gently to ensure that the entire surface of the channels and valves was covered completely. A plastic 2x3 inch block was aligned and placed over the wafer, as shown in *Figure 2.8*. The 5:1 PDMS, described previously in *section 2.3.3*, was poured over the wafer inside the block. The entire assembly was placed into an 80°C oven to cure for 15 min.

Figure 2.8: Model displaying the general setup to create a PDMS cast of an SU-8 pneumatic valve master mold.

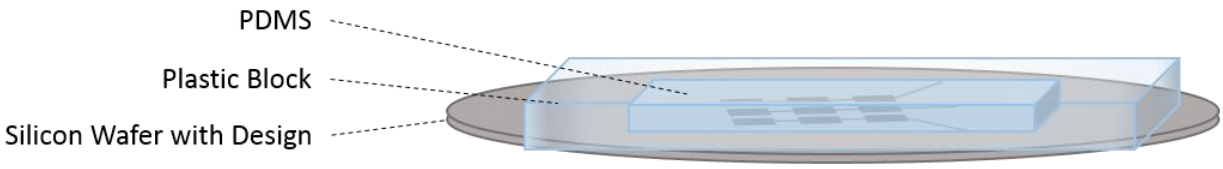

Meanwhile, 1-2 drops of the HMDS:Xylenes solution was placed on the AZ-P4620 fluidic channel master mold to completely cover the channels. The 30:1 PDMS, described previously, was poured into the center of the AZ-P4620 fluidic channel master mold wafer and spin-coated under nitrogen gas for 30 s at 2000 rpm and 1270 rpm/s, resulting in a layer of PDMS approximately 30 µm thick. The wafer was baked at 80°C for 1.5 hrs. Once the fluidic channel wafer was placed in the oven, the 15 min period for the SU-8 2010 master mold was complete. The 10:1 PDMS, described previously in *Table 2.1*, was then used to fill the remainder of the block to the top. (The leftover 10:1 PDMS was saved for later use.) The assembly was then returned to the 80°C oven to bake for another 1.25 hr.

Once a total of 1.5 hr had passed, both the fluidic channel and pneumatic valve molds and casts were removed from the oven and allowed to cool to room temperature (~22°C) inside a positive pressure clean hood. Using a disposable scalpel, the plastic block and PDMS cast of the pneumatic pumping valve mold were removed. Air inlet valves were punched into the PDMS cast of the pneumatic valves using a one millimeter biopsy punch (punched from the channel/valve impression side), as shown by the circular regions in *Figure 2.5B*. The pneumatic valve PDMS cast was aligned and placed carefully over the fluidic channel cast (still attached to the AZ master mold wafer), avoiding air bubbles between the two layers. The leftover ≈10:1 PDMS, discussed previously, was then poured around the pneumatic valve cast to cover any remaining or exposed 30:1 PDMS on the fluidic channel cast, ensuring a tight seal between the fluidic and actuation layers and allowing the 30 µm fluidic layer to be more easily removed after baking. A visual representation for this setup can be seen in *Figure 2.9.* The entire assembly was then placed into an 80°C oven for 1.5 hr.

Figure 2.9: Depiction displaying the final steps in alignment and sealing of the multilayer PDMS microfluidic flow cytometry device.

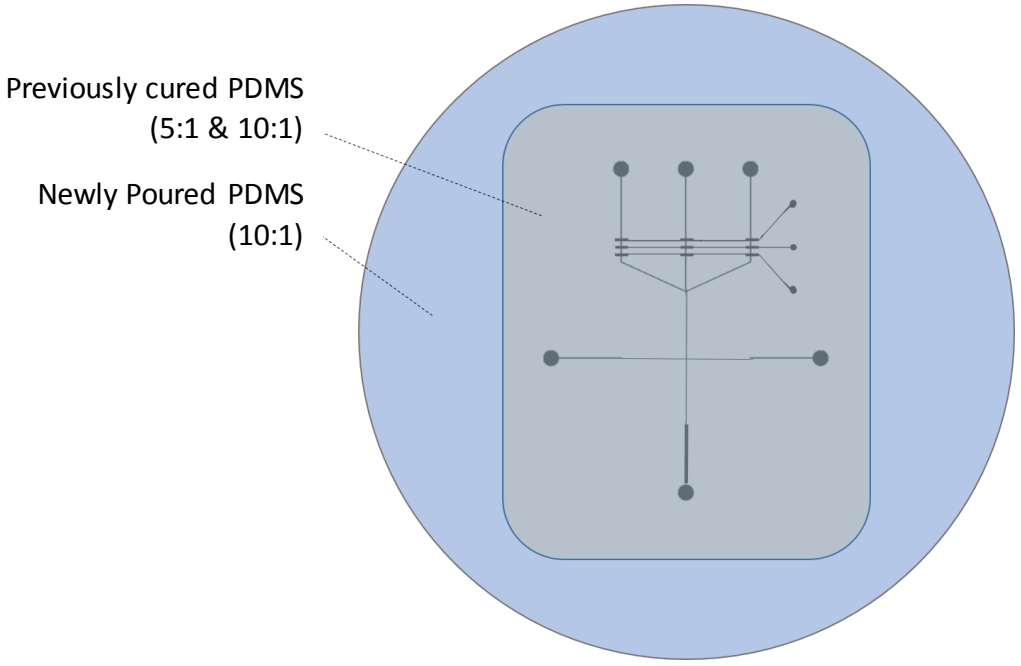

After the final 1.5 hr bake time, the entire assembly was removed from the oven and placed into a positive pressure clean hood to cool to room temperature (~22°C). Meanwhile, a 2x3 inch glass slide (new) was rinsed with ethanol and dried with nitrogen gas at approximately 150 kPa and propped up in the positive pressure clean hood to keep from collecting dust and debris. Once the PDMS cast assembly was fully cooled to room temperature, the layered PDMS cast was carefully peeled from the AZ-P4620 fluidic channel master mold. Fluid reservoirs were punched (from the channel impression side of the PDMS) using a three millimeter biopsy punch in the areas represented by circles in *Figure 2.5A*. For the adjusted design shown in *Figure 2.1B*, the fluid reservoirs were punch in the areas shown in *Figure 2.10*, represented by circles.

Figure 2.10: Depiction of fluid reservoir alignment in an adjusted fluid channel design.

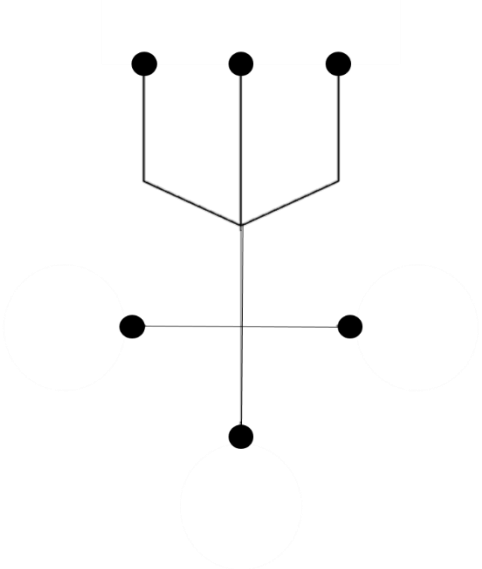

Clear "Magic Tape" (3M) was used to remove any dust and debris from the PDMS cast and glass slide. The PDMS cast was then carefully laid onto the clean 2x3 inch glass slide from one end to another (to avoid air bubbles) with the 30:1 PDMS against the glass slide. A disposable scalpel was then used to cut away excess PDMS, leaving room on the top and bottom of the device for tape to be placed in order to keep the fully assembled device in place during cell analysis. The fully assembled device is shown in *Figure 2.11*.

Figure 2.11: Actual fully assembled multilayer PDMS microfluidic flow cytometry device.

Devices were stored in the same manner as described previously for the AZ-P4620 and SU-8 2010 master molds. The used AZ-P4620 master mold was rinsed with 18 MOhm water and dried with nitrogen gas at less than 50 kPa and stored as previously described. The excess PDMS was carefully removed from the SU-8 2010 master mold using a razor blade and fiber-free cloth with ethanol, then rinsed with 18 MOhm water and dried with nitrogen gas at less than 50 kPa and stored in the same manner as the AZ-P4620 master mold.

2.4 Cell Preparation

2.4.1 Human T-Lymphocyte (Jurkat) Cells

2.4.1.1 Cell Run Buffer Preparation

A cell running buffer was prepared containing 0.20% Tween 20 (w/v), 20% acetonitrile (v/v), 2% bovine serum albumin (BSA) (w/v), 25 mM sodium tetraborate, and 2 mM sodium dodecyl sulfate (SDS) with a total volume of 50 mL, diluted with 18 MOhm water in a 50 mL volumetric flask. Exact amounts used were: 100.00 mg Tween 20, 10.00 mL acetonitrile, 1.00 g BSA, 28.838 mg SDS, and 12.50 mL of 100 mM sodium tetraborate. The pH of this buffer was 8.85 and the conductivity was approximately 14 µS/cm.

2.4.1.2 Carboxyfluorescein diacetate (CFDA) Fluorescent Dye Uptake

The Carboxyfluorescein diacetate (CFDA) was removed from a -20°C freezer and allowed to thaw in a dry bath incubator calibrated to 37°C. Approximately 3 mL of house-cultured human T-lymphocyte (Jurkat) cells were placed into a 15 mL sterile conical tube on put in the same dry bath incubator at 37°C. Three 1 mL sterile Eppendorf tubes were also placed in the dry bath incubator at 37°C, along with two conical tubes containing approximately 6.0 mL each of sterile 1X phosphate buffered saline (PBS). When all components had been equilibrated to 37°C, 95 µL of sterile 1X PBS and 5 µL of CFDA was combined in a warmed (to 37°C) 1 mL Eppendorf tube, vortexed at speed 2 for approximately 15-20 s, and returned to the dry bath incubator to re-equilibrate to 37°C. One milliliter of the Jurkat cells were transferred to one of the warmed 1 mL Eppendorf tubes and spun down at 1100 rpm for 4 min. The supernatant was removed, and

the entire solution of CFDA/PBS was added. The tube was flicked gently to incorporate the cells into the CFDA/PBS solution by breaking up the cell pellet, without causing so much agitation that cells would become damaged. This mixture was left in the dry bath incubator at 37°C for 20 min to allow the uptake of the CFDA into the nucleus of the cells.

Once the CFDA uptake was complete, the cells were visibly bright green in color, but opaque. The cell/CFDA/PBS mixture was diluted to 1 mL with the sterile 1X PBS at 37°C, then spun down at a rate of 1100 rpm for 4 min. The supernatant was removed, then the pellet was diluted with 1X sterile PBS and spun down in the same manner twice more in order to reduce background noise caused by extraneous CFDA not taken up by the cells. Finally, after all wash steps were complete, the cell pellet was re-suspended, using the gentle flicking method mentioned previously, in 1 mL of sterile 1X PBS at 37°C and stored in the dry bath incubator at 37°C until use. Once all experimentation was complete, all components of cell preparation, particularly those which had come into contact with the cells, were soaked in a 10% Clorox bleach solution for 15-20 min before being rinsed down the drain (liquids) or disposed of in the trash (solids).

2.4.2 Human Breast Cancer Cells and Circulating Tumor Cells (CTCs)

Human SUM159PT breast cancer cells (Asterand – Detroit, MI) were obtained from the lab of Dr. Anna Zolkiewska at Kansas State Universtiy (Manhattan, KS) once all cell culturing and staining had been completed. The cells were cultured as recommended by Asterand. A doxycycline-inducible expression of "TurboFPs" red fluorescent protein (Evrogen Joint Stock Co. – Moscow, Russia) was done using the expression vector GIPZ Lentiviral shRNA (Dharmacon, Inc. – Lafayette, CO). The cells were delivered, fully stained, on ice, then warmed to 37°C and diluted with 1X PBS to perform the analysis using the microfluidic flow cytometry device. A whole blood sample collected from mice injected with human SUM159PT breast cancer cells (Asterand – Detroit, MI) was also provided by the Zolkiewska group at Kansas State University and tagged using the same red fluorescent protein as described above. The sample was diluted to a 1:4 solution using 1X PBS (whole blood:PBS) to be run through the microfluidic flow cytometry device.

2.5 Single Cell Analysis and Apparatus

2.5.1 Human Breast Cancer Cell and CTC Analysis

Single cell analysis of the cultured human breast cancer cells and whole blood CTCs was performed using the microfluidic flow cytometry device described previously. Detection was done using a single point detection system. A solid-state 532 nm laser was reflected off a mirror and directed through the microfluidic flow cytometry device approximately 50-100 µm downstream of the channel cross, then shone through a 40X objective lens (WD: 0.6 mm; NA: 0.65) to narrow the beam width and focus it in the center of the microfluidic detection channel. The 30 mW laser beam then passed through a dichroic beam splitter in order to simultaneously obtain laser-induced fluorescence and light scatter data. Each separate beam was then passed through a band pass filter and spatial filter before entering a photomultiplier tube set at -900 V. The amplifier sensitivity was set to 10 µA/V. An analog to digital converter allowed data to be collected using LabVIEW software. This same software was used to precisely control the integrated pneumatic pumping valves which utilized house air at a pressure of 1.50 bar above atmospheric pressure. Data was collected using a data acquisition rate (DAQ) of 800 Hz. A model of the single-point detection apparatus can be seen in *Figure 2.12*.

Figure 2.12: Single-point detection apparatus used for identification of cultured human breast cancer cells and whole blood circulating tumor cells (CTCs).

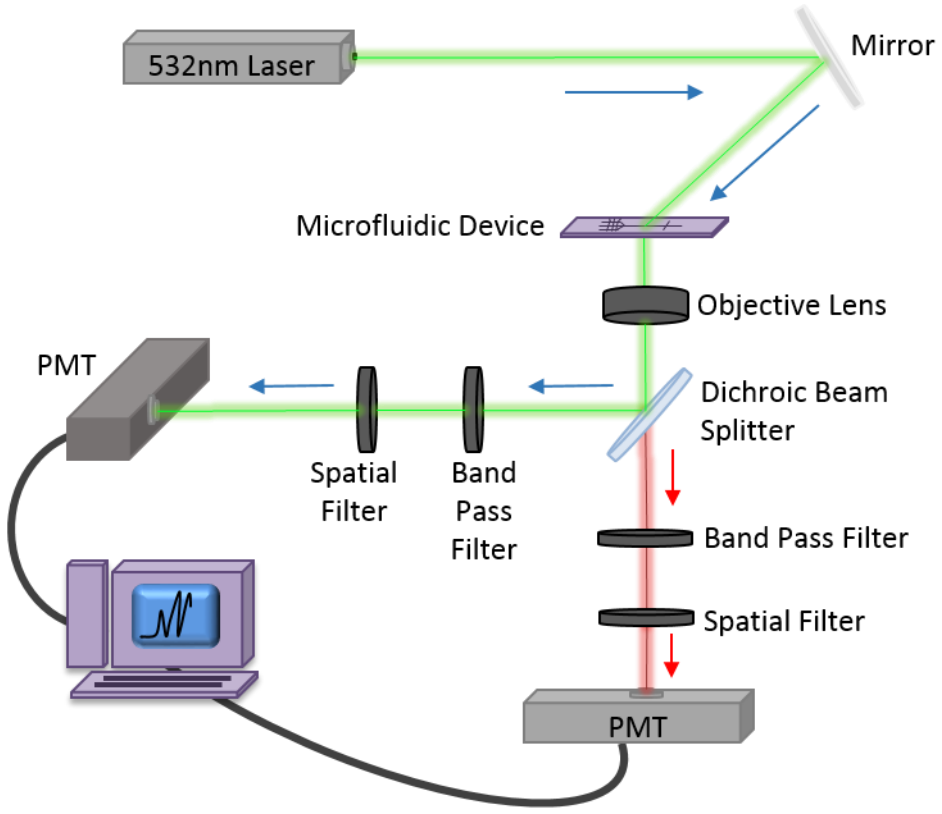

2.5.2 T-Lymphocyte (Jurkat) Cell Analysis for Device Characterization

Single cell analysis of human T-lymphocyte (Jurkat) cells was done for the purpose of overall device functionality characterization. A multi-line argon ion laser was used to detect Jurkat cells labeled with CFDA (carboxyfluorescein diacetate). The 250 mW laser emitted six different wavelengths from 457 nm – 514 nm which was then passed through a prism to redirect to the light and split it into its individual wavelengths. A pinhole was then used to specifically select an excitation wavelength of 488 nm. A series of mirrors were then used to direct the light through an excitation filter and into a dichroic beam splitter. The light was directed through an objective lens to focus the light on the sample within the device. The beam was placed approximately 50-100 µm downstream of the channel cross. The resulting fluorescence emission of the cells was 510 nm. This fluorescence emission was then directed back through the dichroic beam splitter and passed through an emission filter for 510 nm and a notch filter

for 488 nm to help reduce noise by blocking any stray light from the excitation beam. The light was finally directed into a PMT set to -900 V. The amplifier sensitivity was set to 10 µA/V. An analog to digital converter allowed data to be collected using LabVIEW software. This same software was used to precisely control the integrated pneumatic pumping valves which utilized house air at pressures of 0.50 – 2.00 bar above atmospheric pressure. Data was collected using a DAQ of 1000 Hz. A model of the detection apparatus can be seen in *Figure 2.13*.

Figure 2.13: Detection apparatus used for identification of human T-lymphocyte (Jurkat) cells via LIF.

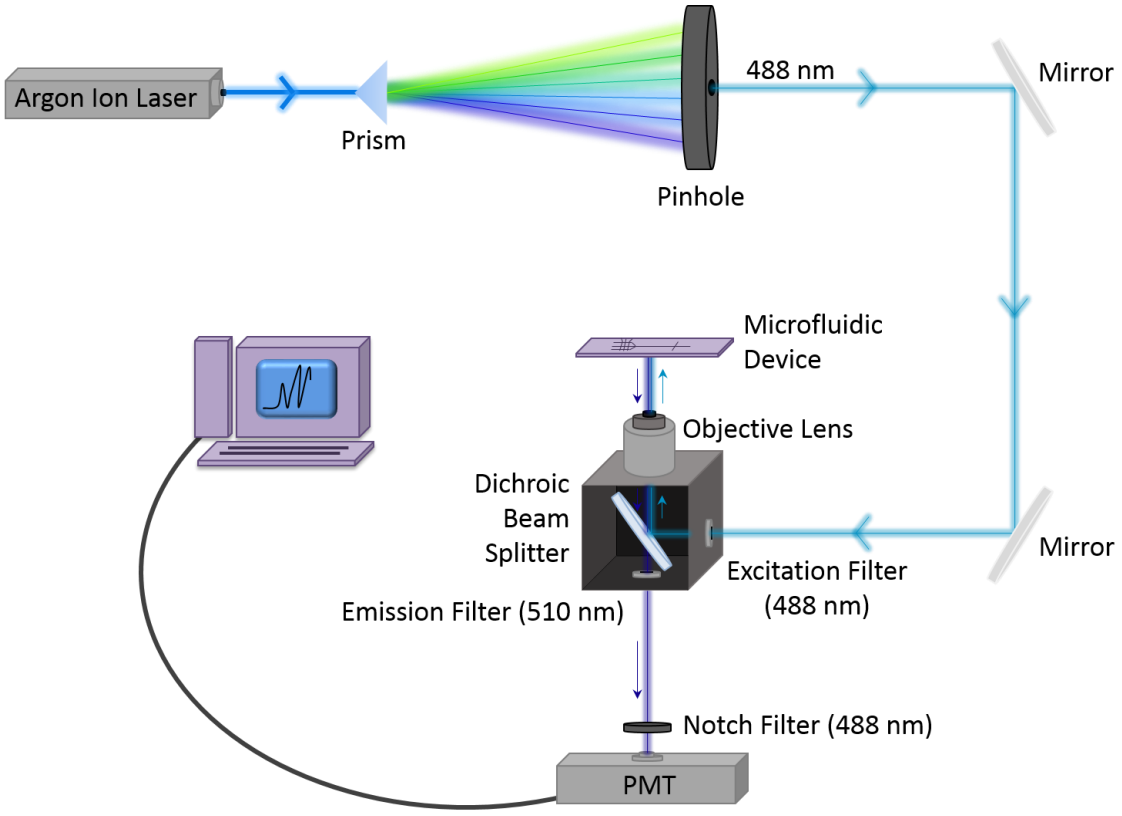

Chapter 3 - RESULTS AND DISCUSSION

3.1 Device Characterization

The device characterization was done using CFDA-labeled human T-lymphocyte (Jurkat) cell, as described previously in *section 2.4.1*. Approximately 50 µL of cells were loaded into the sample reservoir of the device. Cells were run through the device at several different pneumatic valve pumping pressures in order to determine the maximum and optimal pumping speeds. *Figure 3.1* shows the cell loading procedure and direction of cell flow. Visualization of the cells was performed approximately 50-100 µm downstream of the channel cross via laser-induced fluorescence (LIF) by a 488 nm argon ion laser beam, as described in *section 2.5.2*, again shown in *Figure 3.1*.

Figure 3.1: Visual model providing depiction of cell loading, sample flow, and sample visualization.

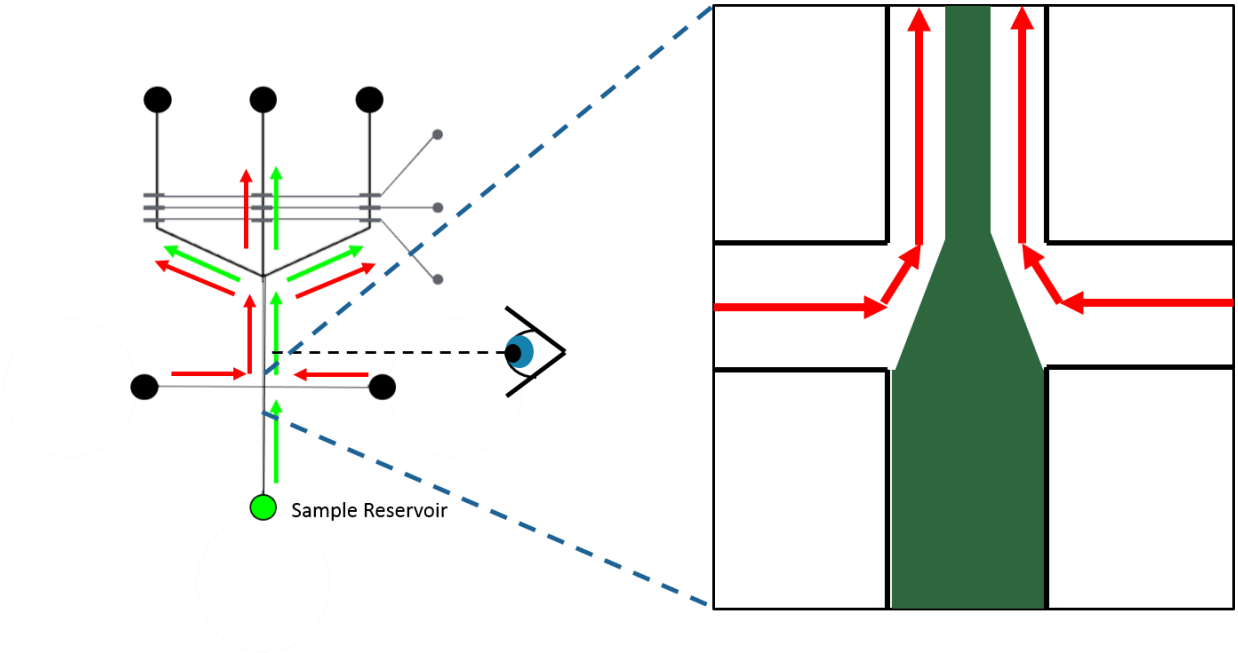

Pneumatic valve pumping pressures from 0.50-2.00 bar (above atmospheric pressure) were used to evaluate the proper valve pressure to be used. The raw data of these runs is shown in *Figures 3.2 - 3.5(A-C)*. The data from pressures at 1.75 bar and 2.00 bar are not shown since the

data was inconclusive. Proper valve actuation was unachievable at these high pressures due to the valves sticking to the fluidic channels, resulting in little-to-no fluid flow. Each run was done for 1000 s with a 10 ms waiting period between individual pumping actuations. Data was collected at a rate of 1000 Hz.

Figure 3.2: Raw LIF data collected from CFDA-labeled Jurkat cells at a pneumatic valve pumping pressure of 0.5 bar and a data acquisition rate (DAQ) of 1000 Hz. Shown at full (A) 1000 s experiment time, and also expanded to (B) 200 s and (C) 10 s.

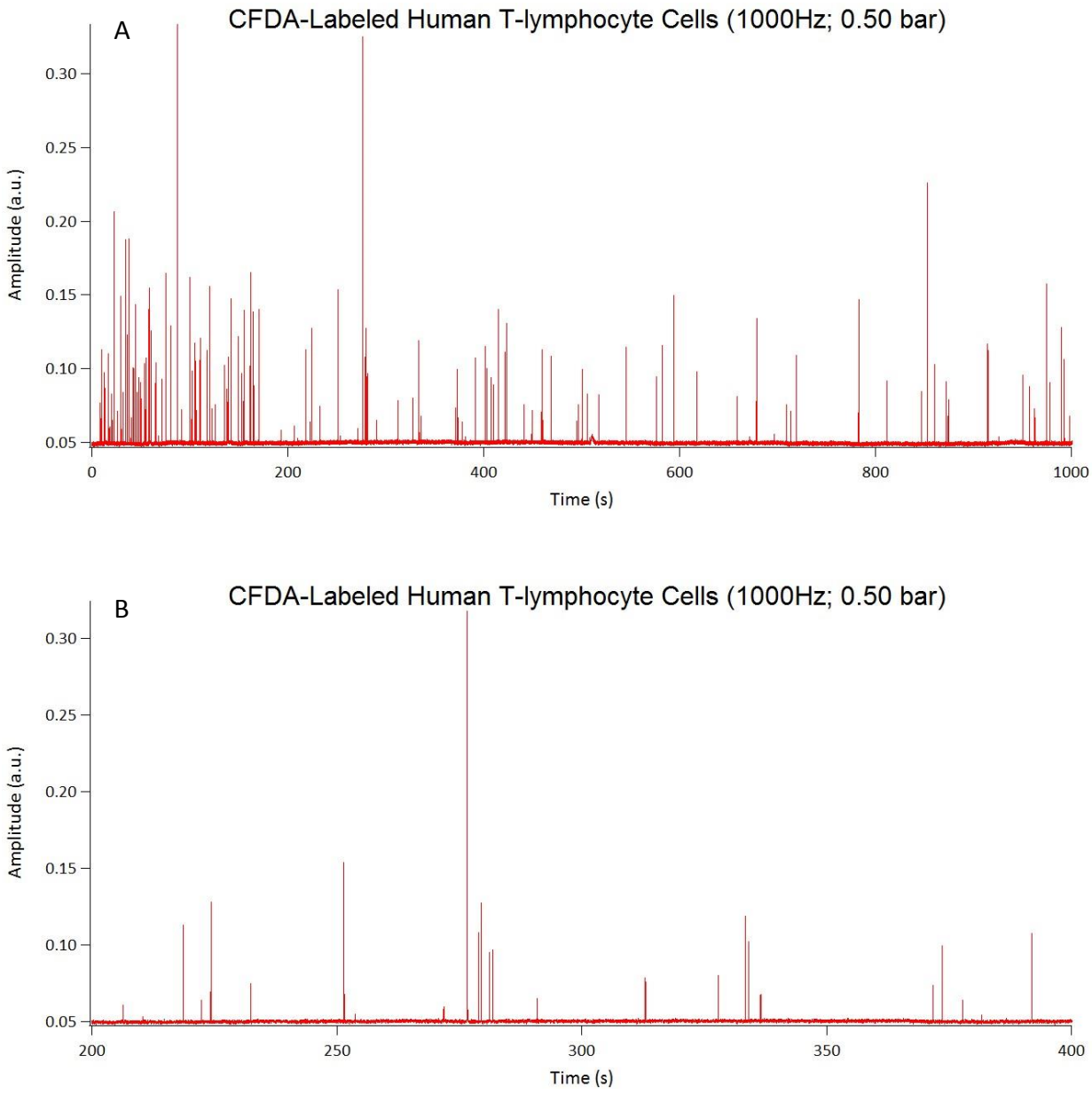

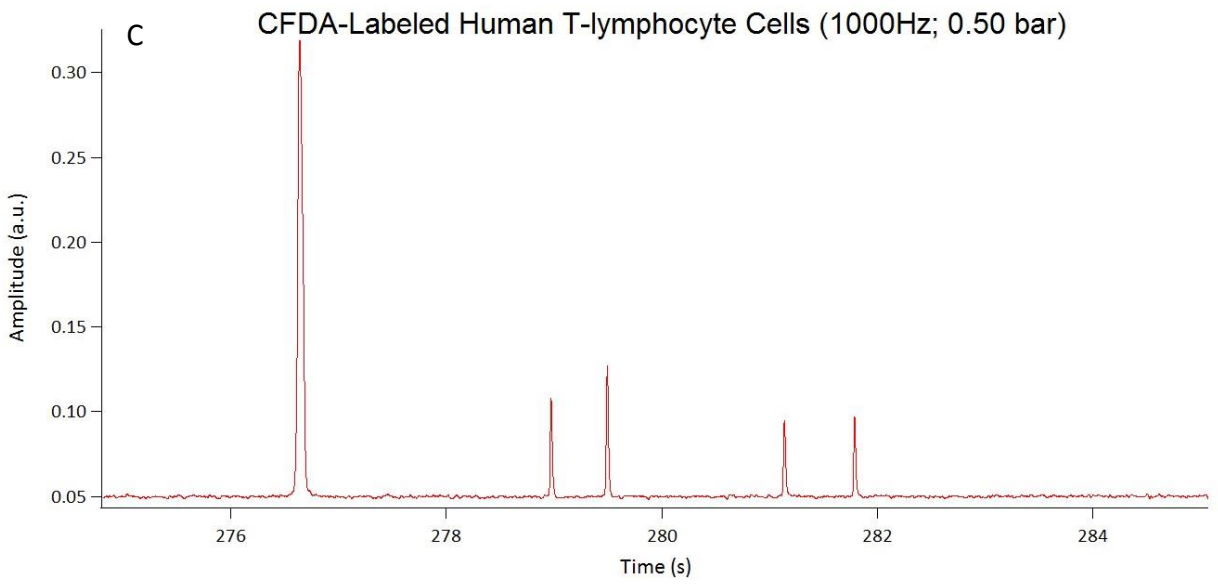

Figure 3.3: Raw LIF data collected from CFDA-labeled Jurkat cells at a pneumatic valve pumping pressure of 1.0 bar and a data acquisition rate (DAQ) of 1000 Hz. Shown at full (A) 1000 s experiment time, and also expanded to (B) 200 s and (C) 10 s.

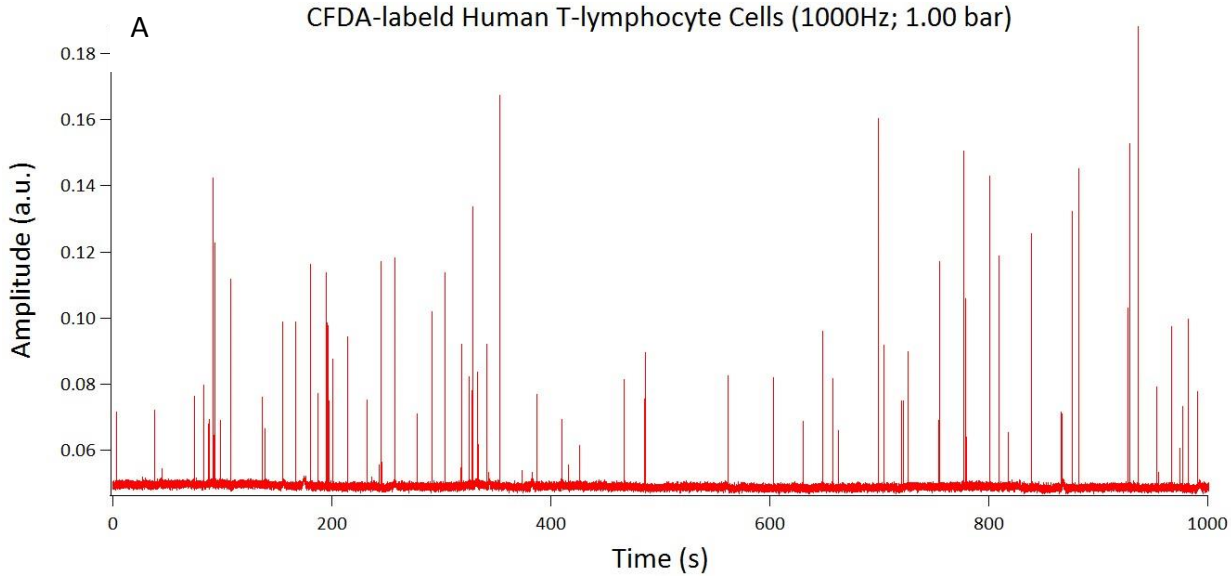

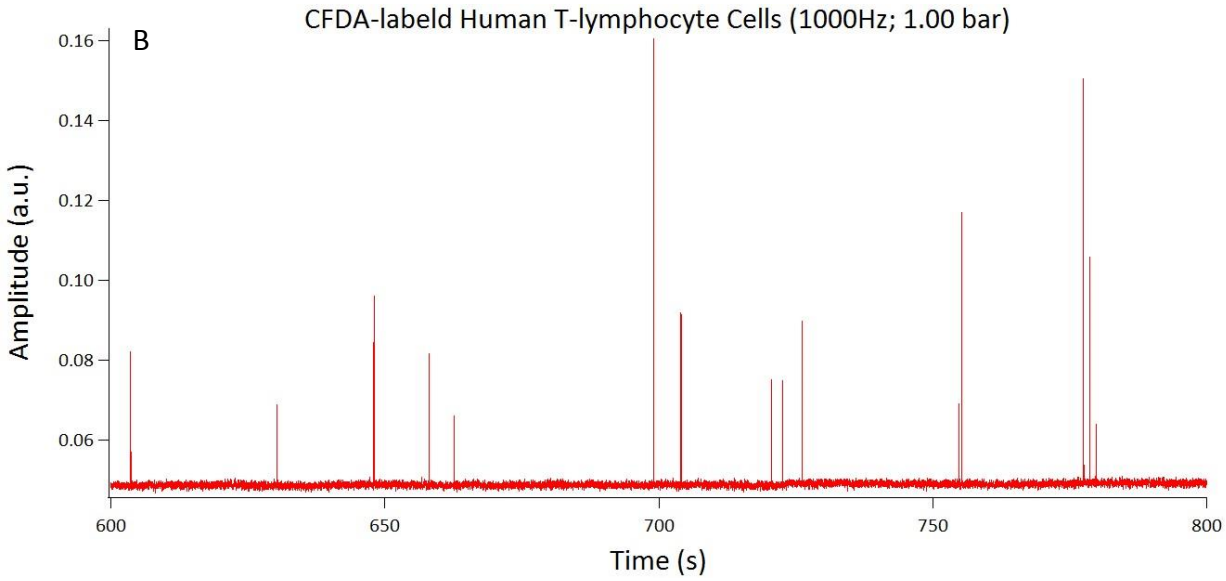
B
CFDA-labeld Human T-lymphocyte Cells (1000Hz; 1.00 bar)
Amplitude (a.u.)
0.16
0.14
0.12
0.10
0.08
0.06
600
650
700
750
800
Time (s)

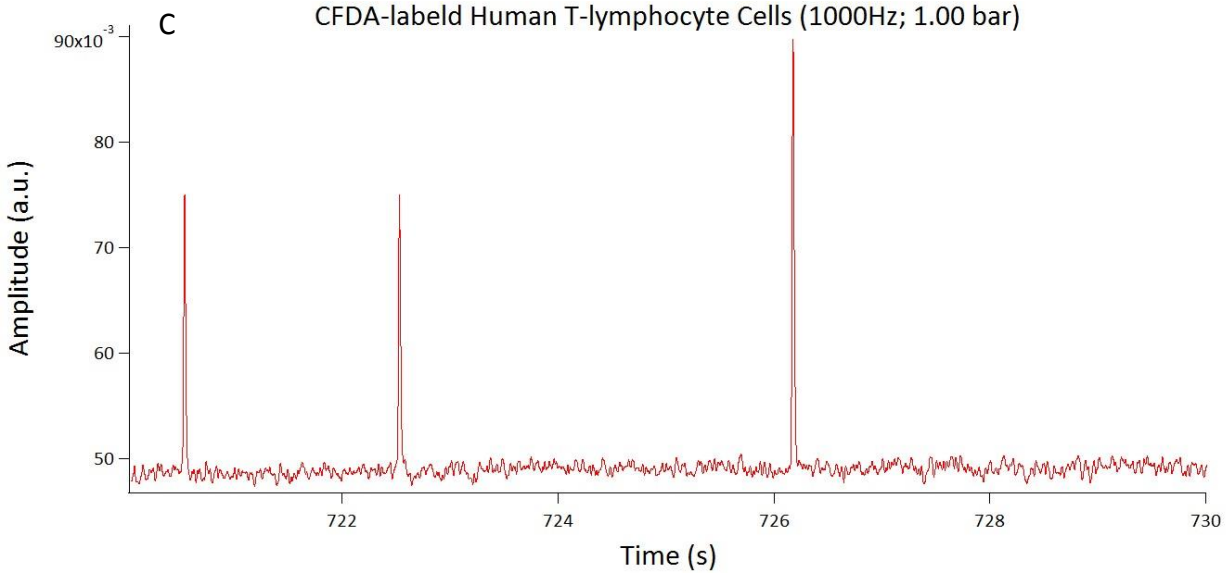
C
CFDA-labeld Human T-lymphocyte Cells (1000Hz; 1.00 bar)
Amplitude (a.u.)
90x10-3
80
70
60
50
722
724
726
728
730
Time (s)

Figure 3.4: Raw LIF data collected from CFDA-labeled Jurkat cells at a pneumatic valve pumping pressure of 1.25 bar and a data acquisition rate (DAQ) of 1000 Hz. Shown at full (A) 1000 s experiment time, and also expanded to (B) 200 s and (C) 10 s.

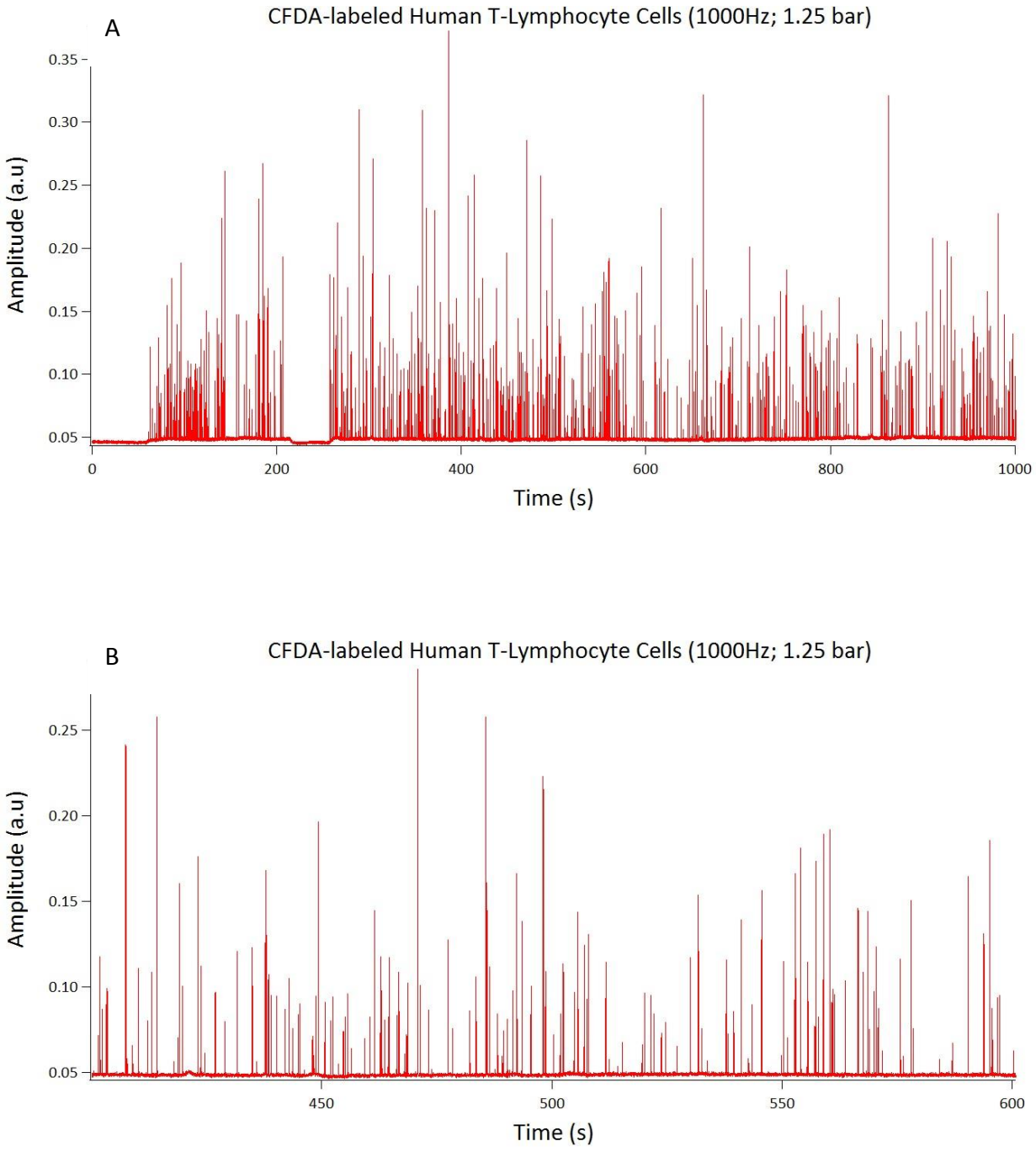

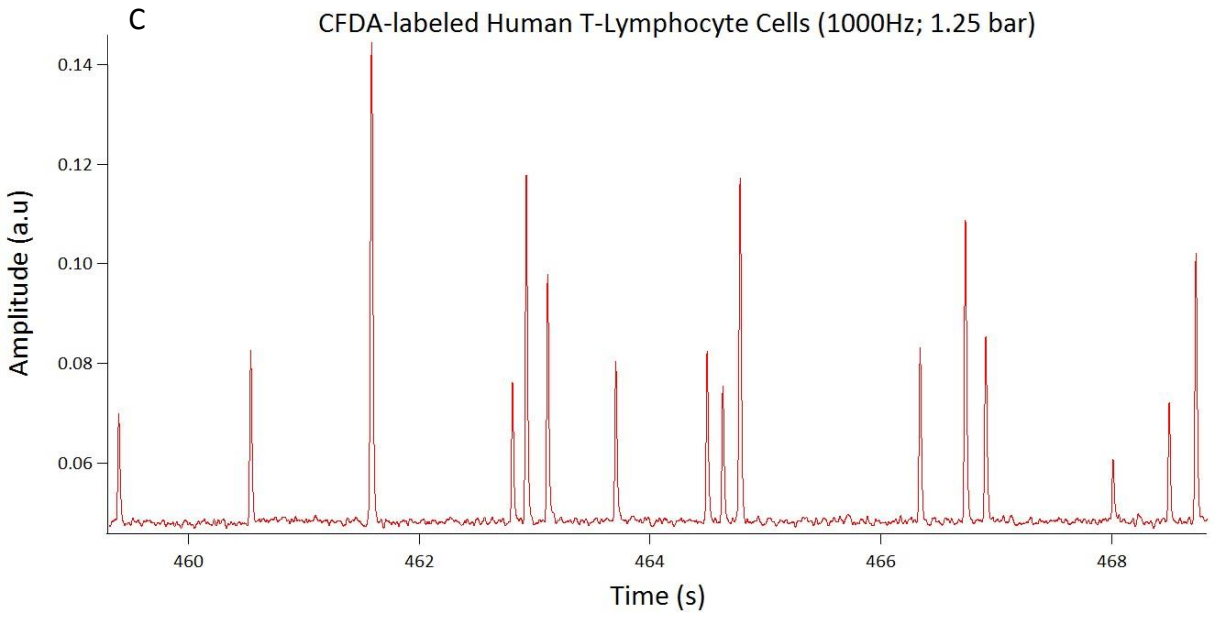

Figure 3.5: Raw LIF data collected from CFDA-labeled Jurkat cells at a pneumatic valve pumping pressure of 1.50 bar and a data acquisition rate (DAQ) of 1000 Hz. Shown at full (A) 1000 s experiment time, and also expanded to (B) 10 s and (C) 3 s.

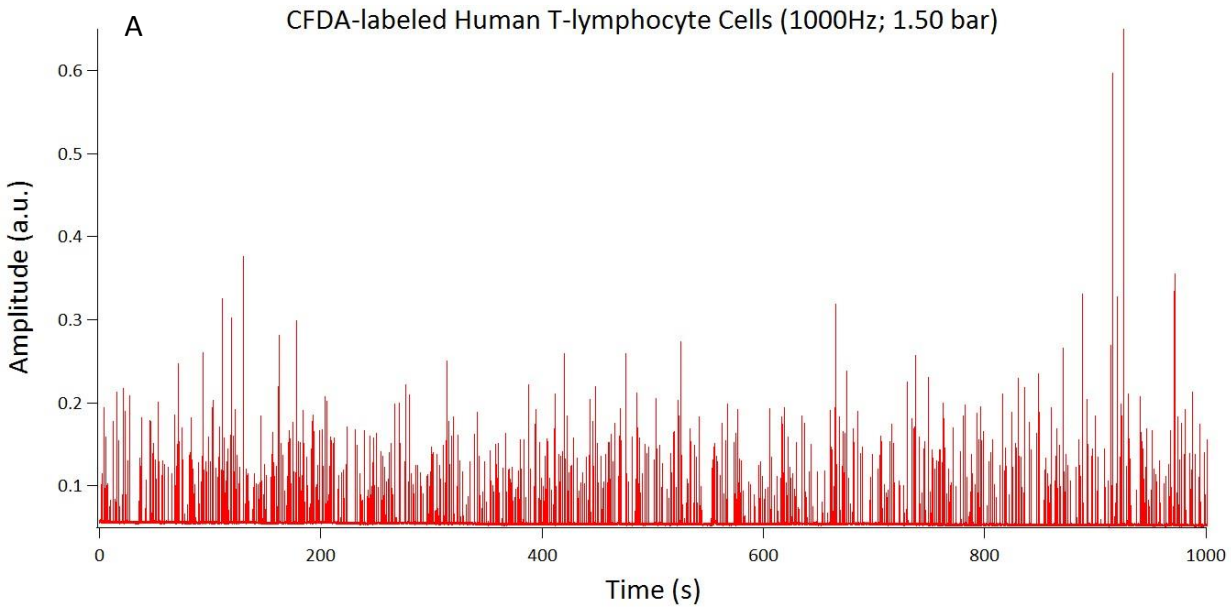

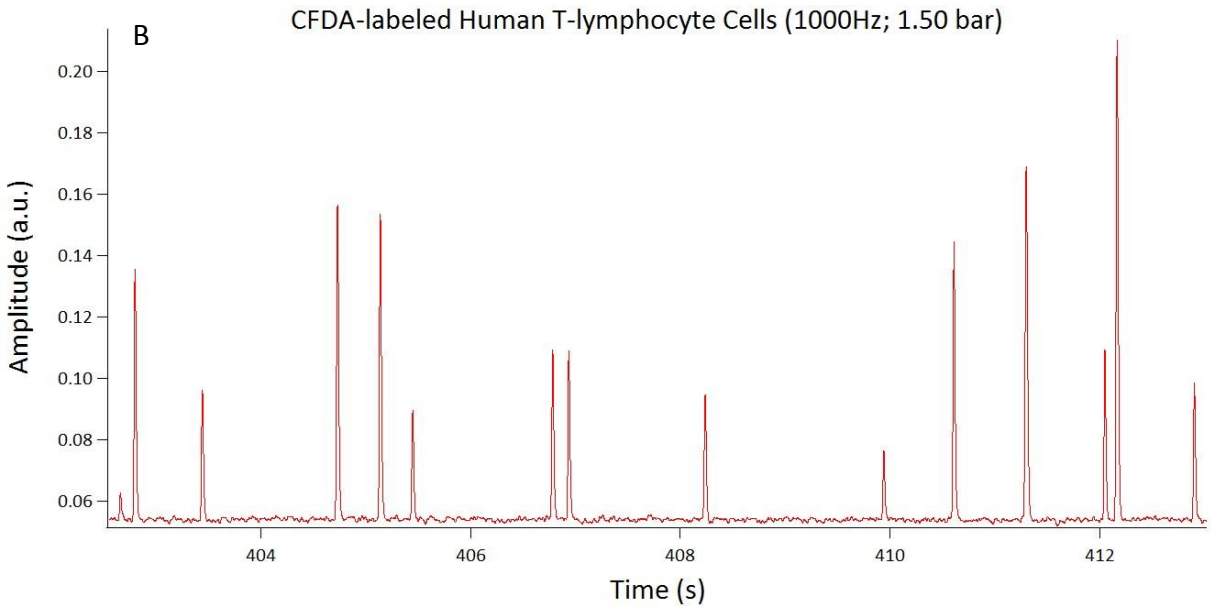

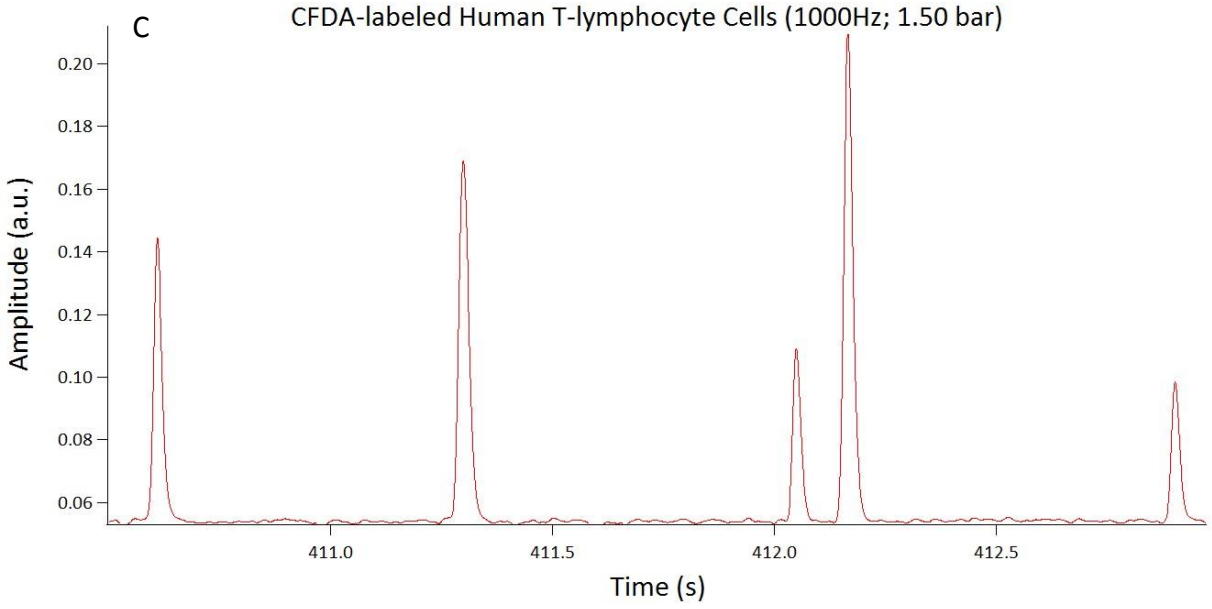

It was expected that higher pneumatic valve pumping pressure would increase the rate at which cells moved through the device, and therefore increase the total number of cells which could be analyzed in a given time period. This was found to be true, as expected. However, at pumping pressures of approximately 1.75 bar or greater it was found that pumping actuation and flow rate significantly decreased due to the actuation valves sticking to the fluidic channels.

It was determined, therefore, that a pressure of 1.50 bar was optimal for pneumatic valve actuation. The collective data displaying this conclusion is shown in *Figure 3.6*.

Figure 3.6: Pneumatic valve pressure comparison displaying the optimum valve pressure.

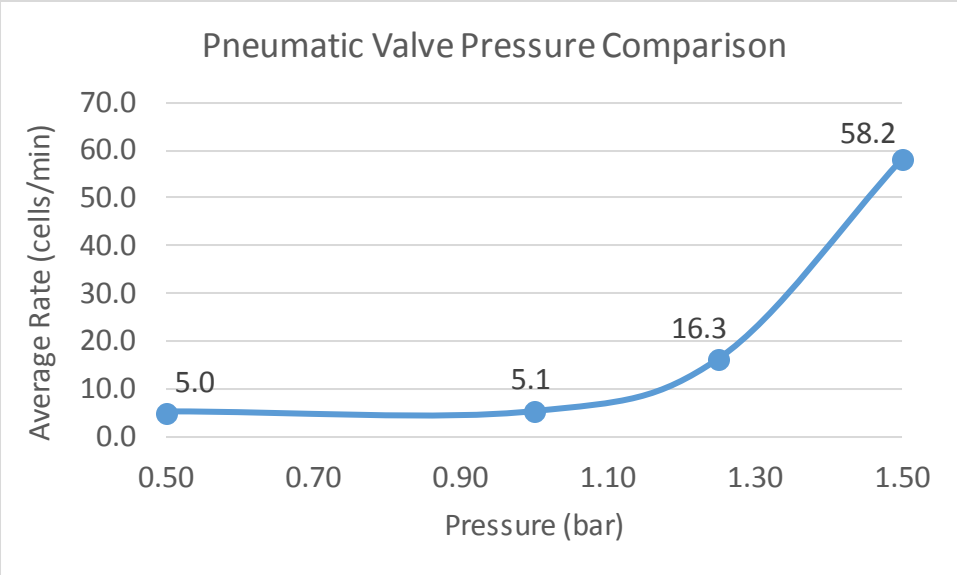

3.2 Human Breast Cancer Cell and CTC Analysis Results

Human SUM159PT breast cancer cells were obtained from the lab of Dr. Anna Zolkiewska of Kansas State University (Manhattan, KS) and arrived pre-tagged and fluorescently labeled with red fluorescent protein. Approximately 50 µL of cells were loaded onto the device, as shown in *Figure 3.1*, and analyzed using the single point detection setup described in *section 2.5.1* and shown in *Figure 2.12*. The sample of cancer cells provided was homogenous. Therefore, ideally the peaks for the laser-induced fluorescence (LIF) data and light scattering (LS) data would align completely. This is because since LIF detects specifically the labeled cancer cells, and LS detects all cells and particles that flow past the detector, if no contamination was present and all cells were properly stained cancer cells, the peaks should correlate. The raw data obtained from this experiment is shown in *Figure 3.7(A-C)*, below.

Figure 3.7: Raw data from single point detection of human breast cancer cells using laser-induced fluorescence (LIF) and light scattering (LS) from full (A) 600 s total run, then expanded to approximately (B) 200 s and (C) 10 s.

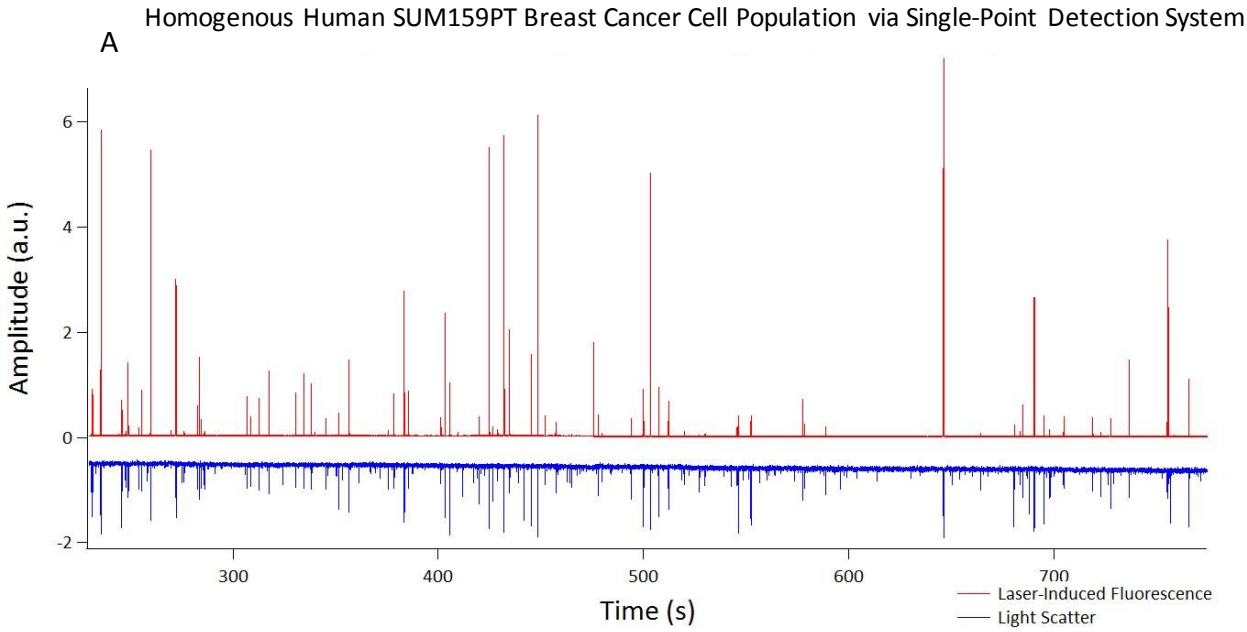

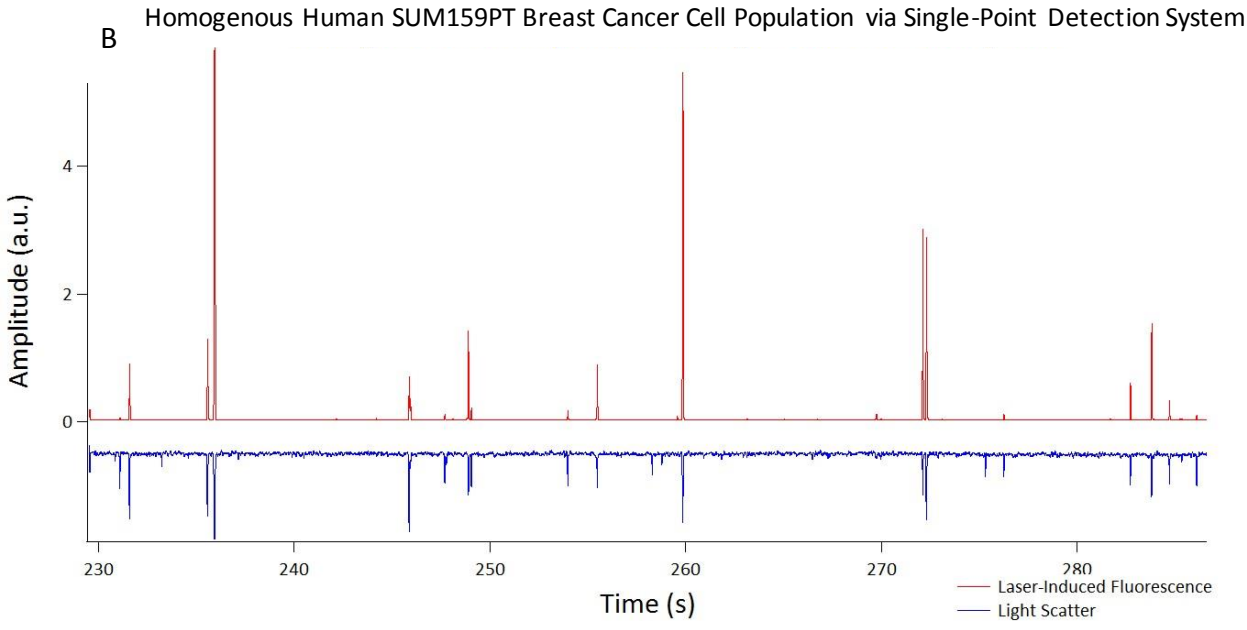

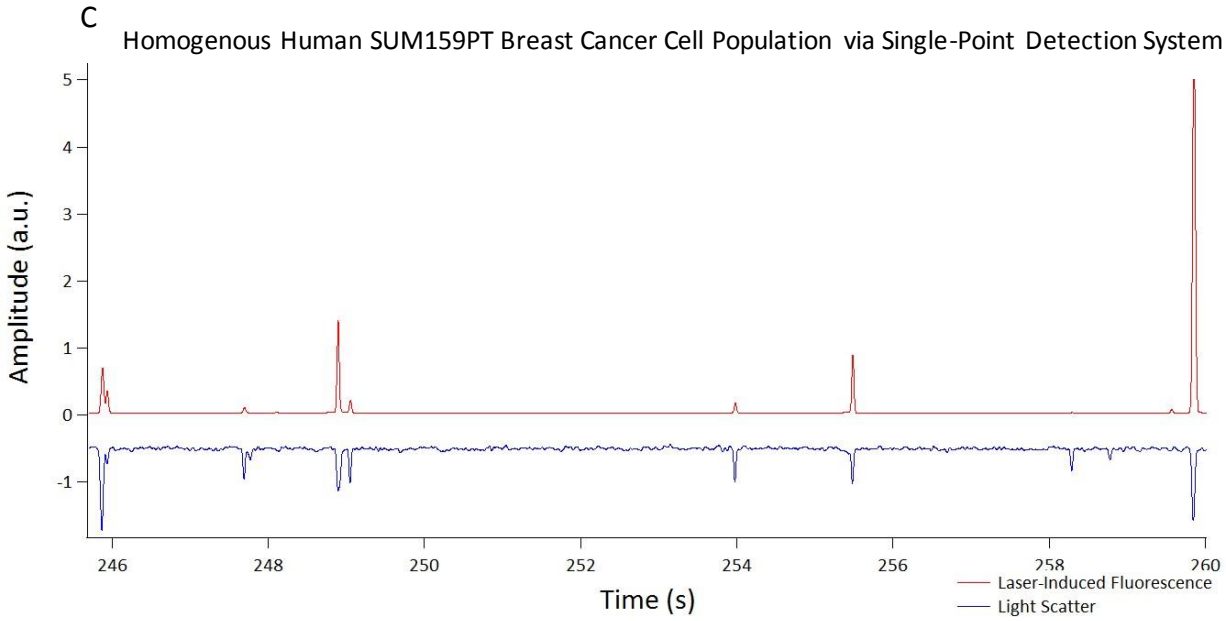

As one can see from the data above, there was a strong correlation between the LIF and LS data. This suggests that indeed, the population was homogenous, and also that the single point detection system was functioning as anticipated. The whole blood sample provided by Dr. Zolkiewska and her team was run in the same manner, as described in section 2.5.1. The raw data is shown in *Figure 3.8(A-C)*.

Figure 3.8: Raw data from single point detection of human CTCs in whole blood grown in mice using laser-induced fluorescence (LIF) and light scattering (LS) from a (A) 20 s run section, then expanded to under (B) 1 s and approximately (C) 0.03 s.

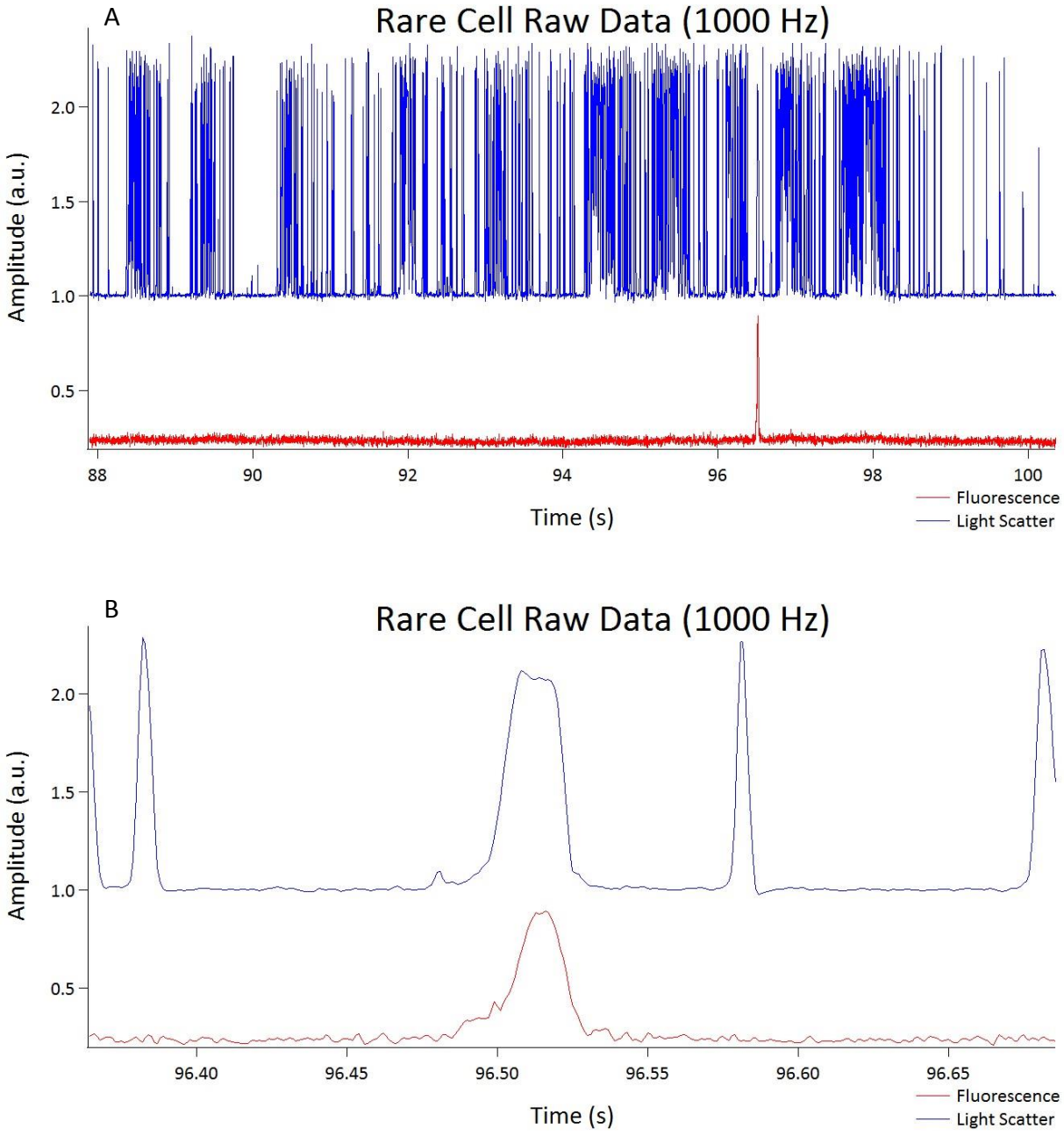

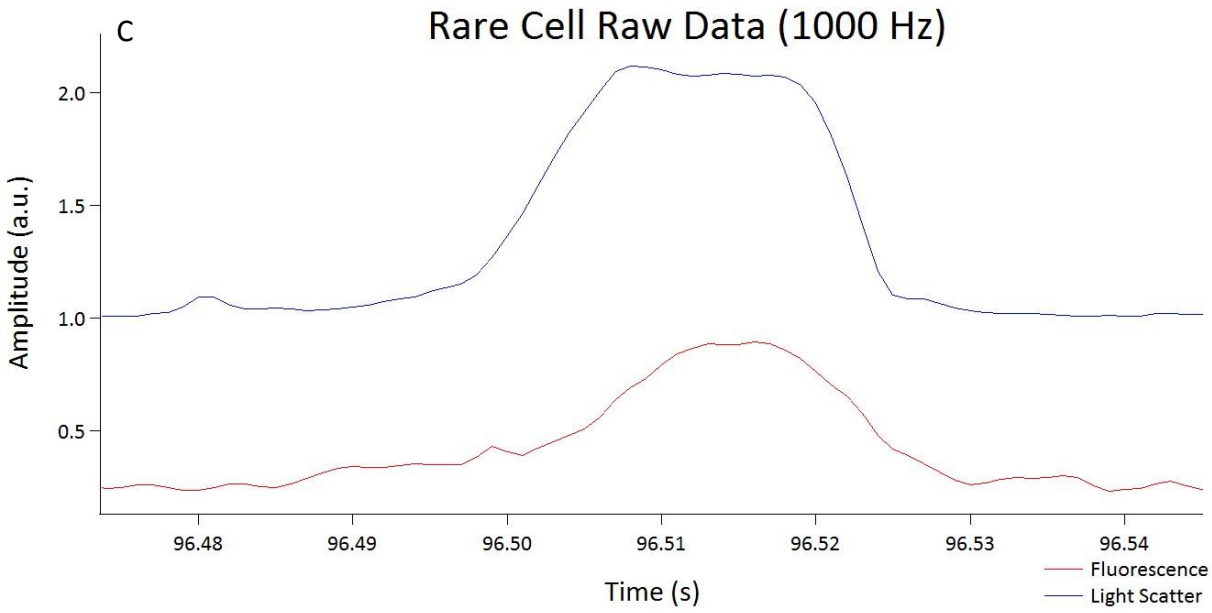

As one can see from the above data, a single circulating tumor cell was detected using the single-point detection apparatus previously described in *section 2.5.1*. Although this may not seem significant, recall that the concentration of circulating tumor cells within the blood can be as low as one in one million. These results demonstrate the high sensitivity and selectivity of the device and method proposed herein. The entirety of the previously discussed data displays the ability to rapidly and simultaneously count a population of cells while also identifying a particular type of cell. This shows great promise for the ability to identify and characterize ADAM12 protease-tagged CTCs in a whole blood sample. *Figure 3.8* shows a histogram representing the distribution of peak amplitudes for the Jurkat cells used during device characterization. Since peak amplitude is also an indicator of cell size, the figure also displays the cell size distribution. As one can see, the distribution is relatively Gaussian, as expected.

Figure 3.9: Peak amplitude distribution at optimal valve pressure of 1.50 bar for CFDA-labeled Jurkat cells.

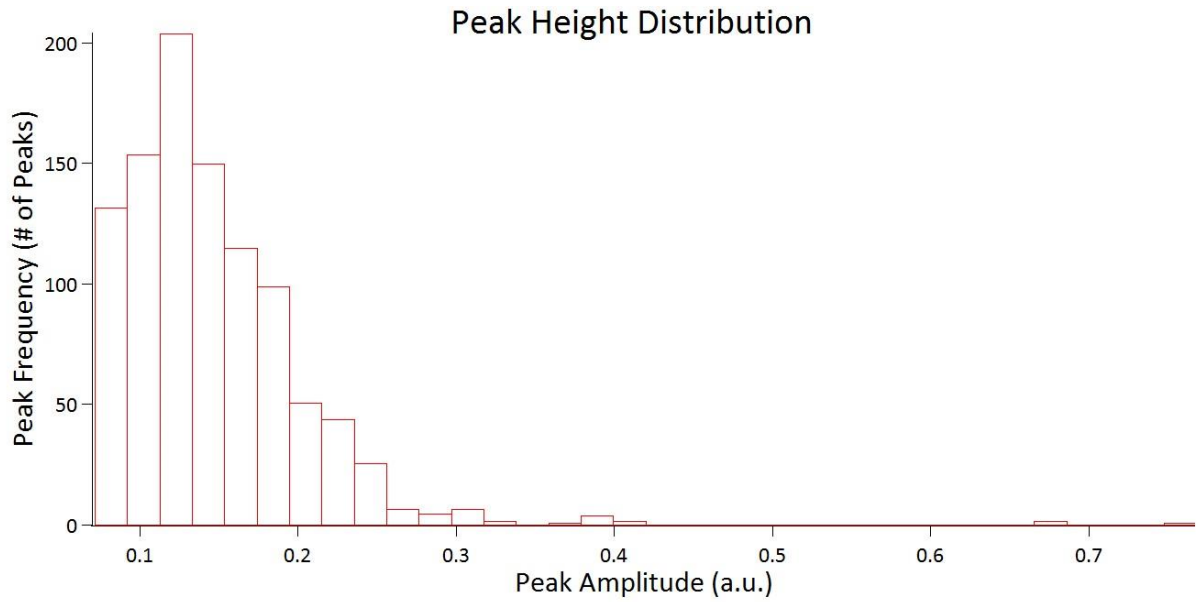

Although the peaks showed a correlation between the fluorescence and light scattering peak positions, demonstrating that the fluorescence and light scattering data was occurring together, the peak amplitudes demonstrated less alignment. This is most likely due to an incorrect adjustment in signal sensitivity. The correlation for the peak position is shown in *Figure 3.10* and demonstrates good linear correlation between peak positions, as expected. The correlation of the peak amplitudes for the fluorescence and light scattering data is shown in *Figure 3.11*.

Figure 3.10: Fluorescence versus light scatter signal position data correlation.

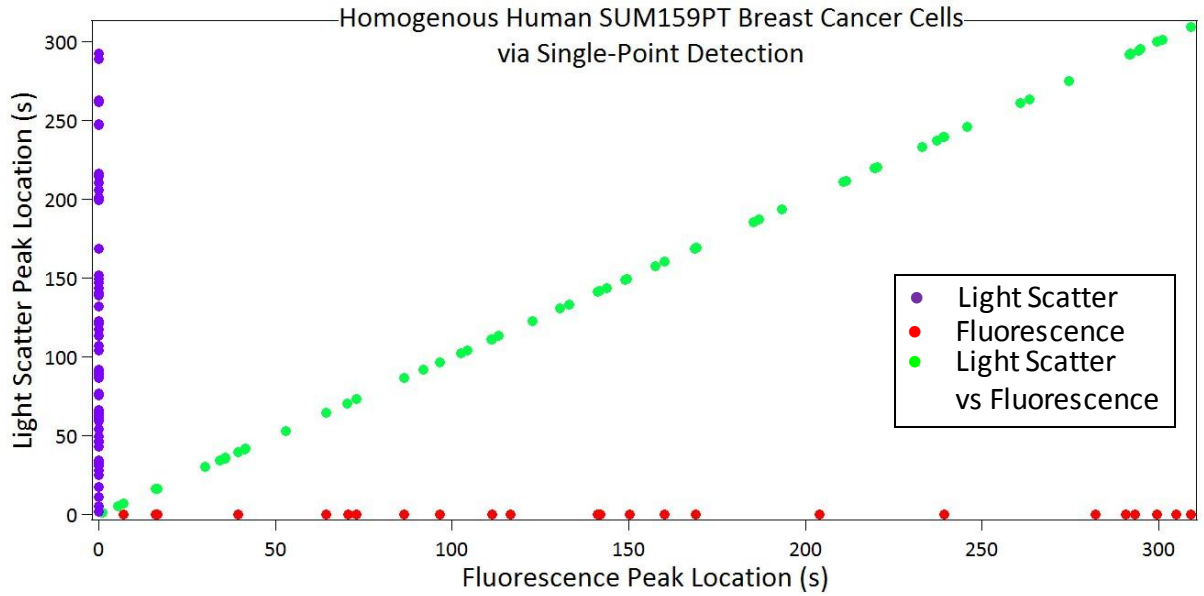

Figure 3.11: Fluorescence versus light scatter signal amplitude data correlation.

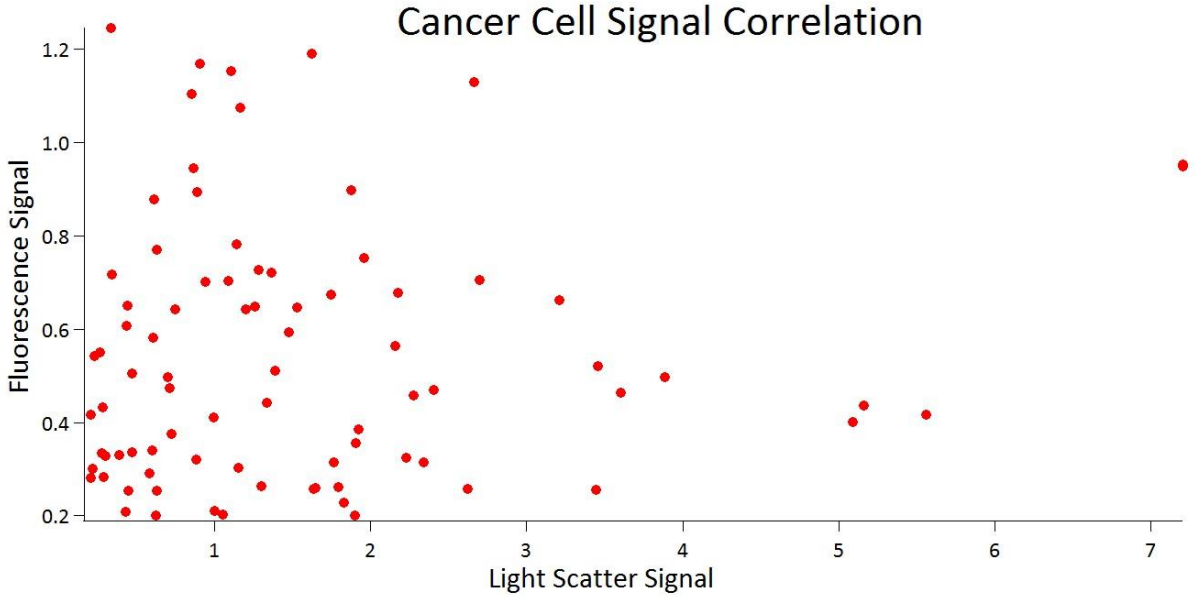

3.3 Conclusion

A multilayer device was successfully fabricated in a rapid, facile, and inexpensive manner. As proof of principle, human Jurkat (T-lymphocyte) cells were analyzed at a rate of approximately 100 cells/min using laser-induced fluorescence. Individual cells were differentiated, displaying an ability to rapidly analyze and characterize individual cells. A pure batch of human

SUM159PT breast cancer cells was analyzed using a single-point detection apparatus, simultaneously obtaining laser-induced fluorescence and light scattering data. Correlation between the fluorescence and light scattering data was observed, indicating the fluorescently-labeled tumor cells were being identified (via fluorescence) and counted (via light scattering) simultaneously. Finally, a single circulating tumor cell was detected within a whole blood sample using the single-point detection system previously described, successfully distinguishing it within the whole blood population. This preliminary data suggests the ability to rapidly and successfully identify and characterize circulating tumor cells within a heterogeneous cell population.

3.4 Future Endeavors

The previously presented data suggests great promise in the ability to detect specific CTC types within a heterogeneous cell population. Therefore, the logical next step in this work would be to test the device and system using a heterogeneous cell population containing a known concentration of CTCs, and compare the experimental results with the known CTC concentration. Further, a similar study should also be performed testing the ability to identify and distinguish various types of CTCs within a cell population. Each type of CTC should be uniquely tagged and fluorescently labeled using their unique ADAM proteases. Additionally, different wavelength lasers, or possibly white light coupled with a prism and/or beam splitter, could be used to detect the LIF of each type of CTC at their own specified wavelengths.

The true long-term goal for this project should be to develop a portable system to be coupled with the device to allow point-of-care analysis for cancer patients. The device would allow multiple individual types of CTCs with various ADAM proteases to be identified simultaneously, ideally within 15 min or less, thereby allowing a more rapid, selective and sensitive method of cancer screening. This would mean earlier cancer detection, more accurate prognosis, more effective treatment methods, and therefore a greater chance of patient survival.

References

1. Longfellow, H. W. In *Introduction;* The Song of Hiawatha; G. Routledge & Co.: London, **1856**; pp 5-9.
2. Macey, M. G. *Flow Cytometry: Principles and Applications;* Humana Press: Totowa, New Jersey, **2007**; , pp 289.
3. Piyasena, M. E.; Graves, S. W. The intersection of flow cytometry with microfluidics and microfabrication. *Lab Chip* **2014***, 14*, 1044-1059.
4. Ng, H.; Smith, D. J.; Nagley, P. Application of Flow Cytometry to Determine Differential Redistribution of Cytochrome c and Smac/DIABLO from Mitochondria during Cell Death Signaling. *PLoS ONE* **2012***, 7*, e42298.
5. Gaforio, J.; Serrano, M.; Algarra, I.; Ortega, E.; de Cienfuegos, G. Phagocytosis of Apoptotic Cells Assessed by Flow Cytometry Using 7-Aminoactinomycin D. *Cytometry* **2002***, 49*, 8-11.
6. Vignon, C.; Debeissat, C.; Georget, M.; Bouscary, D.; Gyan, E.; Rosset, P.; Herault, O. Flow Cytometric Quantification of All Phases of the Cell Cycle and Apoptosis in a Two-Color Fluorescence Plot. *PLoS ONE* **2013***, 8*, e68425.
7. Coleman, W. B.; Tsongalis, G. J. *Molecular Diagnostics;* For the Clinical Laboratorian; Humana Press: New York, **2005**; Vol. 2, pp 246.
8. Clark, S.; Thompson, K. C.; Keevil, C. W.; Smith, M. *Rapid Detection Assays for Food and Water;* International Conference on Developments in Rapid Diagnostic Methods: Water and Food; Royal Society of Chemistry: Cambridge, **2001**; Vol. 272, pp 237.
9. Chew, S. L.; Or, M. Y.; Chang, C. X. L.; Gehring, A. J.; Bertoletti, A.; Grotenbreg, G. M. Stability Screening of Arrays of Major Histocompatibility Complexes on Combinatorially Encoded Flow Cytometry Beads. *Journal of Biological Chemistry* **2011***, 286*, 28466-28475.
10. Mi, Y.; Li, K.; Liu, Y.; Pu, K.; Liu, B.; Feng, S. Herceptin functionalized polyhedral oligomeric silsesquioxane – conjugated oligomers – silica/iron oxide nanoparticles for tumor cell sorting and detection. *Biomaterials* **2011***, 32*, 8226-8233.
11. van Gaal, E. V. B.; Spierenburg, G.; Hennink, W. E.; Crommelin, D. J. A.; Mastrobattista, E. Flow cytometry for rapid size determination and sorting of nucleic acid containing nanoparticles in biological fluids. *J. Controlled Release* **2010***, 141*, 328-338.

12. Wang, M.; He, H.; Turko, I. V.; Phinney, K. W.; Wang, L. Quantifying the Cluster of Differentiation 4 Receptor Density on Human T Lymphocytes Using Multiple Reaction Monitoring Mass Spectrometry. *Anal. Chem*. **2013***, 85*, 1773-1777.

13. Chakraborty, D.; Chakraborty, S. In *Microfluidic Transport and Micro-Scale Flow Physics: An Overview;* Chakraborty, S., Ed.; Microfluidics and Microfabrication; Springer US: New York, **2010**; pp 1-85.

14. Chung, T. D.; Kim, H. C. Recent advances in miniaturized microfluidic flow cytometry for clinical use. *Electrophoresis* **2007***, 28*, 4511-4520.

15. Chou, H.; Spence, C.; Scherer, A.; Quake, S. A microfabricated device for sizing and sorting DNA molecules. *Proc. Natl. Acad. Sci. U. S. A.* **1998***, 96*, 11-13.

16. McClain, M. A.; Culbertson, C. T.; Jacobson, S. C.; Allbritton, N. L.; Sims, C. E.; Ramsey, J. M. Microfluidic Devices for the High-Throughput Chemical Analysis of Cells. *Anal. Chem.* **2003***, 75*, 5646-5655.

17. Poulsen, C. R.; Culbertson, C. T.; Jacobson, S. C.; Ramsey, J. M. Static and Dynamic Acute Cytotoxicity Assays on Microfluidic Devices. *Anal. Chem.* **2005***, 77*, 667-672.

18. Studer, V.; Giao Hang, V.; Pandolfi, A.; Ortiz, M.; Anderson, W. F.; Quake, S. R. Scaling properties of a low-actuation pressure microfluidic valve. *J. Appl. Phys.* **2004***, 95*, 393-398.

19. Thorsen, T.; Maerkl, S. J.; Quake, S. R. Microfluidic Large-Scale Integration. *Science* **2002***, 298*, 580-584.

20. Groisman, A.; Enzelberger, M.; Quake, S. R. Microfluidic Memory and Control Devices. *Science* **2003***, 300*, 955-958.

21. Scanlon, T. C.; Dostal, S. M.; Griswold, K. E. A high-throughput screen for antibiotic drug discovery. *Biotechnol. Bioeng.* **2014***, 111*, 232-243.

22. Zhao, M.; Wei, B.; Chiu, D. T. Imaging multiple biomarkers in captured rare cells by sequential immunostaining and photobleaching. *Methods* **2013***, 64*, 108-113.

23. Smith, J. P.; Barbati, A. C.; Santana, S. M.; Gleghorn, J. P.; Kirby, B. J. Microfluidic transport in microdevices for rare cell capture. *Electrophoresis* **2012***, 33*, 3133-3142.

24. Lee, A.; Park, J.; Lim, M.; Sunkara, V.; Kim, S. Y.; Kim, G. H.; Kim, M.; Cho, Y. All-in-One Centrifugal Microfluidic Device for Size-Selective Circulating Tumor Cell Isolation with High Purity. *Anal. Chem.* **2014**, *86*, 11349-11356.

25. Alberts, B.; Bray, D.; Hopkin, K.; Johnson, A. D.; Johnson, A.; Lewis, J.; Raff, M.; Roberts, K.; Walter, P. *Essential Cell Biology;* Garland Science: New York, 2009; Vol. 3, pp 860.

26. Baldizon Cells. *http://www.mckenziejrhigh.com/7th-grade-life-science.html* (accessed March, **2015**).

27. Yap, T. A.; Lorente, D.; Omlin, A.; Olmos, D.; de Bono, J. S. Circulating tumor cells: a multifunctional biomarker. *Clin Cancer Res* **2014**, *20*, 2553-2568.

28. Sinha, G. Circulating tumor cells in early-stage breast cancer. *J Natl Cancer Inst.* **2012**, *104*, 1693-1694.

29. Schwartz, A. M.; Nolan, N. Circulating tumor cells: what goes around, comes around. *J Natl Cancer Inst.* **2014**, *106*.

30. Duhachek-Muggy, S.; Li, H.; Qi, Y.; Zolkiewska, A. Alternative mRNA Splicing Generates Two Distinct ADAM12 Prodomain Variants. *PLoS ONE* **2013**, *8*.

31. Li, H.; Duhachek-Muggy, S.; Dubnicka, S.; Zolkiewska, A. Metalloproteinase-disintegrin ADAM12 is associated with a breast tumor-initiating cell phenotype. *Breast Cancer Res Treat* **2013**, *139*, 691-703.

32. Duffy, M.; Mullooly, M.; O'Donovan, N.; Sukor, S.; Crown, J.; Pierce, A.; McGowan, P. The ADAMs family of proteases: new biomarkers and therapeutic targets for cancer? *Clinical Proteomics* **2011**, *8*, 1-13.

33. Cole, M. C.; Desai, A. V.; Kenis, P. J. A. Two-layer multiplexed peristaltic pumps for high-density integrated microfluidics. *Sensors Actuators B: Chem.* **2011**, *151*, 384-393.

34. Unger, M. A.; Chou, H.; Thorsen, T.; Scherer, A.; Quake, S. R. Monolithic Microfabricated Valves and Pumps by Multilayer Soft Lithography. *Science* **2000**, *288*, 113.